



CELL-CELL COUPLING OCCURS IN DORSAL MEDULLARY NEURONS AFTER MINIMIZING ANATOMICAL-COUPLED ARTIFACTS

J. B. DEAN,* R.-Q. HUANG,† J. S. ERLICHMAN,‡ T. L. SOUTHARD
and D. T. HELLARD

Department of Physiology and Biophysics, Wright State University, School of Medicine,
College of Science and Mathematics, Dayton, OH 45435 U.S.A.

Abstract—Dye (Lucifer Yellow) and tracer (Biocytin) coupling, referred to collectively as anatomical coupling, were identified in 20% of the solitary complex neurons tested in medullary tissue slices (120–350 µm) prepared from rat, postnatal day 1–18, using a modified amphotericin B-perforated patch recording technique. Ten per cent of the neurons sampled in nuclei outside the solitary complex were anatomically coupled. Fifty-eight per cent of anatomically coupled neurons exhibited electrotonic postsynaptic potential-like activity, which had peak-to-peak amplitudes of ≤ 7 mV, with the same polarity as action potentials; increased and decreased in frequency during depolarizing and hyperpolarizing current injection; was maintained during high Mg^{2+} -low Ca^{2+} chemical synaptic blockade; and was measured only in anatomically coupled neurons. The high correlation between anatomical coupling and electrotonic postsynaptic potential-like activity suggests that Lucifer Yellow, Biocytin and ionic current used the same pathways of intercellular communication, which were presumed to be gap junctions. Anatomical coupling was attributed solely to the junctional transfer of Lucifer Yellow and Biocytin since potential sources of non-junctional staining were minimized. Specifically, combining 0.26 mM amphotericin B and 0.15–0.5% Lucifer Yellow produced a hydrophobic, viscous solution that did not leak from the pressurized pipette tip (≤ 3 µm outer diameter) submerged in artificial cerebral spinal fluid. Moreover, unintentional contact of the pipette tip with adjacent neurons that resulted in accidental staining, another source of non-junctional staining, was averted by continuously visualizing the tip prior to tight seal formation with infrared video microscopy, used here for the first time with Hoffman modulation contrast optics. During perforated patch recording, which typically lasted for 1–3 h, Lucifer Yellow was confined to the pipette, indicating that the amphotericin B patch was intact. However, once the patch was intentionally ruptured at the end of recording, the viscous, lipophilic solution entered the neuron resulting in double labeling. Placing a mixture of amphotericin B, Biocytin and Lucifer Yellow directly into the pipette tip did not compromise tight seal formation with an exposed, cleaned soma, and resulted in immediate (<1 min) steady-state perforation at 22–25°C.

This adaptation of conventional perforated patch recording was termed “rapid perforated patch recording”. The possible functional implication of cell-cell coupling in the dorsal medulla oblongata in central CO_2/H^+ chemoreception for the cardiorespiratory control systems is discussed in the second paper of this set [Huang *et al.* (1997) *Neuroscience* **80**, 41–57]. © 1997 IBRO. Published by Elsevier Science Ltd.

Key words: gap junction, electrotonic coupling, perforated patch recording, nucleus tractus solitarius, dorsal motor nucleus of vagus, brain slice.

Dye coupling refers to the intercellular spread of the fluorescent dye Lucifer Yellow (LY) into one or more

*To whom correspondence should be addressed.

†Present address: Department of Pharmacology, Health Science Center at Fort Worth, UNT, 3500 Camp Bowie Blvd, Fort Worth, TX 76107, U.S.A.

‡Borwell Building, E724, Department of Physiology, Dartmouth Medical School, Lebanon, NH 03756, U.S.A.

Abbreviations: ACSF, artificial cerebral spinal fluid; DMSO, dimethylsulfoxide; DMV, dorsal motor nucleus of vagus; EGTA, ethyleneglycoltetra-acetate; ELPSP, electrotonic postsynaptic potential; HEPES, N-2-hydroxyethylpiperazine-N-2-ethanesulfonic acid; IR-HMC, infrared-Hoffman modulation contrast; LY, Lucifer Yellow; NTS, nucleus tractus solitarius; P, postnatal day; rapid PPR, rapid perforated patch recording; R_{in} , input resistance; τ , membrane time constant; V_m , membrane potential.

adjacent cells after loading it into a single cell with a microelectrode.⁶³ The presumption that dye movement from the recorded cell into its neighbors occurs via gap junctions, and that it denotes electrotonic coupling, is based on electrophysiological and anatomical evidence in neural and non-neural systems.^{23,41,42,46,62,70} In the mammalian CNS, dye coupling alone provides only indirect evidence for electrotonic coupling; however, when care is taken to minimize the artifacts associated with this technique,^{3,21,38} it is a workable alternative for surveying a region for cell-cell coupling compared to the arduous task of recording from cell pairs under blind slice conditions.^{12,39,41,70} It is not surprising, therefore, that dye coupling is often the first line of evidence for gap junctions in a nucleus of the mammalian

CNS,^{2,23,37,41,43,64} and that it is used to study conditions that increase or decrease coupling between central neurons.^{11,26,27,43,48} Recently, biotinylated tracers (Biocytin and Neurobiotin) have also been used to identify gap junctions.^{43,48,67,68} Dye coupling with LY⁶³ and/or tracer coupling using Biocytin⁶⁷ will be referred to collectively in this paper by the more general term, anatomical coupling.^{16,43}

There is always the concern that some proportion of anatomical coupling is an artifact due to the non-junctional transfer of stain since experiments are conducted blindly without visualizing the microelectrode tip and neuron.^{3,20,38} Any LY or biotinylated tracer that leaked from the microelectrode tip into the neuropil could be taken up by transected neuronal processes and damaged cell bodies,^{3,34,48} or internalized by intact neurons through endocytosis.⁶⁹ Staining of multiple neurons could also result from undetected impalements with the microelectrode and unintentional staining;^{3,34} it has also been proposed that the same microelectrode is capable of simultaneously recording, and therefore staining, two neurons.^{1,32} Thus, while it is accepted that anatomical coupling is an indirect measure of gap junctions and electrotonic coupling in the mammalian CNS, the potential for anatomical-coupling artifacts, and the technical limitations that prevent detection when staining artifacts occur, have limited estimates of the amount of cell-cell coupling.^{20,38}

The present study describes techniques that significantly reduce sources of non-junctional staining and applies these techniques to investigate whether neurons in the vicinity of the solitary complex (i.e. nucleus tractus solitarius, NTS, and dorsal motor nucleus of vagus, DMV) are anatomically and electrotonically coupled. Previously, spontaneous sub-threshold potentials with the same polarity as action potentials, but which did not resemble chemical postsynaptic potentials, were observed during blind whole-cell recordings in the solitary complex in transverse slices prepared from weaned and adult rat (unpublished observations in Ref. 18). It was unknown if the source of these small biphasic potentials was dendritic spikes invading the cell body,⁵⁹ ephaptic interactions between juxtapositioned neural membranes^{20,53,54} or electrotonic postsynaptic potentials (ELPSPs).^{23,41,70} The latter scenario, if true, suggests that certain neurons in the solitary complex are electrotonically coupled and may, therefore, exhibit anatomical coupling. To minimize potential sources of non-junctional staining artifacts, the amphotericin B-perforated patch technique⁵¹ was modified to prevent LY and Biocytin leakage from the pipette. Further, both the neuron and the pipette tip were continuously visualized at all stages of the experiment using infrared-Hoffman modulation contrast (IR-HMC) video microscopy. Non-leakage of pipette solution was accomplished in part by placing the antibiotic

directly in the tip, which had the added benefit of permitting steady state perforation within approximately 1 min of forming a tight seal; hence, this variation of the conventional perforated patch recording technique was called “rapid perforated patch recording” (rapid PPR).

To test the hypothesis that cell-cell coupling occurs in the dorsal medulla oblongata, experiments were conducted in transverse brain slices prepared from preweanling rats to address the following questions. (1) Are neurons in and near the solitary complex anatomically coupled under recording conditions that reduce the likelihood of non-junctional dye transfer? (2) Does spontaneous ELPSP-like activity occur in neurons during chemical synaptic blockade? (3) If so, does ELPSP-like activity correlate with anatomical coupling in the same cell?

The second paper³⁰ discusses the effects of CO₂-induced intracellular acidosis on anatomically coupled neurons in the solitary complex and adjoining nuclei. Preliminary accounts of this research have been presented in abstract form.¹⁶

EXPERIMENTAL PROCEDURES

Animals

Eighty-two rats, postnatal day (P) 0–21, and 16 rats (weanling and adult) were used in this study. All animals were purchased from Harlan Sprague-Dawley (Indianapolis, IN, U.S.A.). All efforts were made to minimize animal suffering prior to killing the rat by rapid decapitation according to the *National Institutes of Health Guide for Care and Use of Laboratory Animals*. Preweanling pups ≤ P14 were anesthetized using hypothermia.¹⁴ In rat pups > P14, which cannot be anesthetized using hypothermia, other types of anesthetics were not used because of the reported depressant actions these agents have on neuronal activity⁴⁷ and electrotonic synaptic transmission (see Refs 6, 41, 47 in the following paper³⁰).

Brain slices

All stages of brain dissection and tissue slicing were conducted in ice-cold (approx. 4°C) artificial cerebral spinal fluid (ACSF) of the following composition (in mM): 124 NaCl, 5.0 KCl, 1.3 MgSO₄, 26 NaHCO₃, 1.24 KH₂PO₄, 2.4 CaCl₂ and 10 glucose; 300 mosM and pH ~7.3 after equilibration with 5% CO₂–95% O₂ carbogen gas mixture. A tissue block was prepared that encompassed the mid-pontine level through the upper cervical spinal cord. As in other studies by this laboratory,^{16,18,30,57} transverse medullary slices ranging from 120 to 150 µm (thin slices) and 300–400 µm (thick slices) in thickness were cut with a Vibratome (Pelco 101, Series 1000) from an area beginning at obex and extending rostrally to the rostral end of the hypoglossal nucleus. Slices from preweanlings were submerged in ACSF (22–25°C) aerated with carbogen gas mixture. A slice was transferred to a superfusion chamber with a glass bottom fashioned from a microscope slide coverslip, submerged in ACSF (flowing at ~5 ml/min, 22–25°C), and stabilized with a nylon mesh attached to a platinum wire frame.²¹ Cell bodies were visualized continuously (see below) and cleaned for tight-seal recording by removing the overlying debris of the slice surface using the technique described by Edwards *et al.*²¹ Thick slices from weanlings and adults were submerged in ACSF (~30°C) aerated with carbogen gas mixture. A slice was transferred to a superfusion/interface chamber (flowing at 1–3 ml/min,

35–37°C) and stabilized with a nylon mesh. Cells were recorded blindly without cleaning using the tight-seal technique adapted from Blanton *et al.*⁹

Chemical synaptic blockade medium

High Mg²⁺-low Ca²⁺ synaptic block medium^{15,17} was prepared similarly to control ACSF except that [Mg²⁺] was increased from 1.3 to 11.4 mM, [Ca²⁺] was decreased from 2.4 to 0.2–1.2 mM and [NaCl] was decreased accordingly to maintain osmolarity at ~300 mosM. This superfusion medium blocked both evoked and spontaneous chemical synaptic potentials (not shown).

Unpublished observations made by this laboratory have shown that Ca²⁺ is a major charge carrier for the action potential in many solitary complex neurons in preweanling rats. Consequently, if [Ca²⁺] was decreased below 1.2 mM, it was common for the neuron's membrane potential (V_m) to become unstable. Likewise, spontaneous activity of the neuron sometimes decreased in low Ca²⁺ medium; e.g., Fig. 1 in Huang *et al.*³⁰ The use of 1.2 mM Ca²⁺ minimized these direct effects of low Ca²⁺ on excitability without compromising the effectiveness of the medium for blockade of chemical synaptic transmission in most neurons studied (for an exception see inhibitory postsynaptic potential activity in Fig. 10, below).

Pipette solution and patch pipettes

The internal solution contained (in mM): 130 potassium methanesulfonic acid, 20 KCl, 5 (N-[2-hydroxyethyl] piperazine-N'-[2-ethanesulfonic acid]) (i.e. HEPES) and 1 ethylene glycol-bis(β-aminoethyl ether)N,N,N',N'-tetraacetic acid (i.e. EGTA), adjusted to pH 7.3–7.35 with 10 M KOH and osmolarity set at 290–300 mosM. A stock solution of amphotericin B (Sigma A-4888) in dimethylsulfoxide (DMSO) was prepared (60 mg/ml) and then diluted in the above internal solution to a final concentration of 240 µg/ml (0.26 mM); refer to Rae *et al.*⁵¹ for additional details. LY-CH dipotassium salt (Sigma L-0144) and Biocytin (Sigma B-1758) were added to the amphotericin B-internal solution at a concentration of 0.15–0.5%. This final mixture, which will be referred to in the remainder of the paper as "pipette solution", was filtered (0.2 µm pore-size, Nalgene 176-0020) and used to fill the pipette along its entire length, including the tip. Fresh pipette solution, which was maintained on ice, effectively perforated neuronal membranes for ~3 h once it was prepared from amphotericin B-DMSO stock solution. To test for leakage of pipette solution in the absence of LY-CH dipotassium salt, the water-soluble dye, rhodamine B (Sigma R-6626), was included in the pipette solution so that any solution leaking from the pipette tip could be detected during epifluorescent illumination.

Patch pipettes were fabricated from borosilicate glass (TW150F-6, World Precision Instruments) using a Kopf vertical pipette puller (model 700B). The puller's solenoid was disengaged so that the pipette was produced using a one-stage gravity pull. The tip had an outer diameter of ~2 µm with a slowly tapering shank resembling "electrode B" in Fig. 5 of Rae *et al.*⁵¹ The pipette tip, which was neither heat polished nor coated with Sylgard prior to filling, had a d.c. resistance of 4–6 MΩ.

Electrophysiology

Current-clamp recordings in preweanlings were conducted at room temperature using an Axopatch 1D amplifier (CV-4 headstage, ×1/100 gain; Axon Instruments). Rapid PPRs of neurons in weanlings and adults were made at 35–37°C using an Axoclamp 2A (HS-2 headstage, ×0.1 gain; Axon Instruments). A KCl "DriRef" reference electrode (World Precision Instruments) or Ag–AgCl wire was placed in the slice bath to complete the circuit. Current and V_m were recorded on a four-channel VCR (Vetter Co., model 400). A TL-1/pCLAMP data acquisition system

(Axon Instruments) and 486 personal computer were used for delivering pulsing protocols to neurons. Input resistance (R_{in}) was determined by the slope of the linear regression of current and V_m using 4–6 points over a range from resting V_m (~−55 mV) down to at least −90 mV. All reported resting V_m values were corrected by subtracting the liquid junction potential (+5 mV) plus any measurable offset detected after the pipette was retracted from the cell body. Rapid PPRs were considered acceptable if the neuron had a resting V_m of at least −40 mV and an action potential that passed through 0 mV. Subthreshold potentials were considered as candidates for ELPSPs if they were biphasic and had the same polarity as an action potential. ELPSP-like activity was also tested in high Mg²⁺-low Ca²⁺ chemical synaptic blockade medium and during depolarizing and hyperpolarizing current injection into the recorded neuron.

Visualization of unstained neurons in slices from preweanlings

An upright, fixed-stage microscope (Nikon Optiphot-2UD) with a 12 V-100 W halogen lamp was equipped with standard HMC optics including: Nikon 40× water immersion objective with an internal Hoffman modulator (N.A. 0.55, 2.0 mm working distance), condenser (N.A. 0.5, 18 mm working distance) and contrast-control polarizer. Unstained neurons were visualized either through the binoculars or with a video camera system (Hamamatsu model XC-77 CCD video camera module, C2400 CCD camera control, Sony PVM-122 BW video monitor). The internal dentate mechanism that locks the Nikon F2-trinocular head in either the binocular or CCD camera position was removed so that selection between either position could be achieved with minimal vibration to the microscope, tissue slice and recording pipette. The maximum age was ~P14 for viable thin slices and optimal viewing conditions using conventional HMC microscopy.

Thicker slices and older animals (at least P21) could be used by adapting infrared video microscopy to HMC optics. The video components were similar to those used with differential interference contrast optics;⁶⁵ however, owing to their dissimilar optical components, there were several differences in IR-HMC video microscopy that warrant mentioning. Two infrared cut filters were removed from the optical path: one from the front of the microscope's lamp-house where it attaches to the filter receptacle (42 mm diameter, held in position with a tension ring), and the other from the front end of the XC-77 CCD video camera module (16 mm diameter). The Hamamatsu CCD video camera has a spectral response ranging from 400 to 940 nm without the infrared cut filter. A 45 mm diameter infrared filter (transmission at 700–790 nm, Omega Optical filter no. 770WB40) was placed in the optical path before the HMC condenser. The contrast control polarizer, which was normally positioned before the condenser to vary the contrast and sharpness of the Hoffman image, was not used during infrared illumination because it darkened the image and reduced the allowable thickness of slice that could be used for visualizing neurons. Despite removal of the contrast-control polarizer, a high contrast, three-dimensional Hoffman-like image was still maintained. This phenomenon was determined to be due to oblique illumination of the brain slice, resulting from IR light that was refracted by the slit aperture of the Hoffman condenser, which was of sufficient quantity to be detected by the CCD camera. Recent experiments have shown that the Hoffman 40× water-immersion objective can be replaced with a Nikon 40× CFWI long-working distance objective (2 mm working distance) and still render the same Hoffman-like image during infrared video microscopy. This fact was also attributed to oblique illumination of the brain slice. This was an important finding that greatly increased the light-gathering properties of the imaging system (since there was no longer an internal modulator in the light path) for observing

epifluorescent images in alternation with IR-HMC video microscopy.

Digitized images of neurons and pipette tip location were acquired at high and low magnifications via the CCD camera, frame grabber board and imaging software (ComputerEyes/RT Mono, Digital Vision, Dedham, MA, U.S.A.) and a 486 personal computer.

Epifluorescence microscopy

LY fluorescence in the patch pipette was monitored intermittently using a Nikon epifluorescence attachment with 100 W mercury lamp and Nikon filter cube B-2A. The same unit was used to visualize LY in neurons in whole-mounted slices after fixation. Experiments on dye leakage from the pipette also used Rhodamine B dye and a Nikon G-2A filter cube.

Histology

Lucifer Yellow. After rupturing the amphotericin B-patch (described in the Results), the neuron was dialysed with amphotericin B-solution containing LY and Biocytin for 20–30 min; typically a depolarizing pulse (0.3–0.5 nA × 25 ms) was delivered at 3 Hz to facilitate Biocytin loading. The slice was removed from the recording chamber and fixed by immersion in 4% paraformaldehyde in 0.1 M sodium phosphate buffer solution at 4°C for 24–48 h (pH 7.4). Each fixed slice was cleared in DMSO for 20–30 min at room temperature, whole-mounted and coverslipped in DMSO and viewed using epifluorescent illumination.²⁴ It was possible to remove the coverslip, turn the slice over, and coverslip it again to photograph dendrites coursing through the rostrocaudal extent of the transverse slice. After confirming the cell's location and photographing the LY image, the slice was removed from DMSO (which reversed the clearing process) and placed in 20% glycerol in 0.1 M phosphate-buffered saline at 4°C for three to 120 days.

Biocytin. After LY inspection, double-labeled neurons were solidified for bright-field inspection using the avidin-biotin complex reaction.²⁸ Slices were pretreated with ethanol (50%, 20 min; 70%, 25 min; 50%, 20 min) to suppress endogenous peroxidase activity of red blood cells⁴⁴ and then rinsed (2 × 10 min) in 0.01 M phosphate-buffered saline containing 0.1% Triton X-100 detergent. Tissue slices were incubated in 1:200 avidin-biotin complex (Vector ABC kit, PK-4000) for either 2 h at room temperature with agitation or overnight at 4°C. Slices were rinsed (3 × 5 min and then 1 × 10 min) in 0.01 M phosphate-buffered saline. Tissue slices were then incubated in 20 mg diaminobenzidine and 10 mg nickel ammonium sulfate in 100 ml 0.05 M Tris buffer (pH 7.4) for 5–7 min or until a dark reaction product was seen in the cell with bright-field inspection. Alternatively, the diaminobenzidine substrate kit for peroxidase (SK-4100) was used. Slices were rinsed (7 × 5 min) in 0.01 M phosphate-buffered saline and whole-mounted on to a gelatin-coated slide, air-dried at room temperature and dehydrated in a graded alcohol series (50%, 5 min; 70%, 2 × 5 min; 95%, 2 × 5 min; 100%, 2 × 5 min; xylene, 2 × 5 min). Whole-mounted slices were coverslipped in DPX and air-dried.

More recent experiments, not reported here, have added Vaney's procedure,⁶⁸ which enhances the intensity of staining with Biocytin in neurons of the dorsal medulla. Prior to whole-mounting the slice on the gelatin-coated slide, the slice was placed in 0.02% nitro blue tetrazolium in 0.1 M Tris buffer (pH 8.2) for 5 min, and then exposed to green light fluorescence (Nikon G-2A filter cube) for 2 min.

RESULTS

The findings of this study are presented in three general sections. The first section, divided into three

subsections, gives evidence for non-leakage of pipette solution from the tip, describes the key steps in establishing a rapid PPR and then rupturing the patch to stain the neuron. These technical details are germane to: (i) minimizing sources of non-junctional dye and tracer transfer in anatomical-coupling studies; (ii) increasing the efficiency of PPR by decreasing the time to achieve steady-state perforation; and (iii) enabling double staining for routine morphological analysis after rapid PPR. Consequently, a thorough description of these procedures is given. The second section presents evidence that certain neurons in NTS, DMV and adjacent dorsal medullary nuclei are anatomically coupled. The third section presents evidence that ELPSP-like activity in the dorsal medulla occurs exclusively in anatomically coupled neurons.

Non-leakage of pipette solution

An unanticipated early finding was that pipette solution did not leak from tips that were $\leq 3 \mu\text{m}$ in outer diameter with a corresponding resistance of $>3 \text{ M}\Omega$ (Fig. 1A). The initial pulse of pressure would produce a small cloud of solution containing LY that was visible only momentarily (not shown—this small amount of leakage was not a problem because the tip was $\sim 3 \text{ mm}$ above the surface of the tissue slice at this time and the flow of ACSF instantly removed any pipette solution). No additional dye was observed leaking from the pipette, even with sustained positive pressure of 250 mmHg. The tip was not irreversibly plugged since the slightest suction would immediately draw ACSF into the pipette. Tips $>3 \mu\text{m}$ outer diameter with lower resistances leaked slightly (B), but much less than equivalent pipettes filled with a standard whole-cell pipette solution.¹⁸ If a pipette that did not leak amphotericin B-solution was placed in DMSO, pipette solution began to leak slowly (C). If either amphotericin B or LY was omitted, then pipette solution leaked profusely from the pressurized tip submerged in ACSF (D–F; in the absence of LY, leakage was detected visually by inclusion of water-soluble rhodamine B in the pipette solution). The critical factor for non-leakage, therefore, was the combination of amphotericin B and LY in the pipette solution. The two pipette solutions in (A) (normal) and (D) (minus amphotericin B) were compared using spectrofluorimetry to determine whether the addition of amphotericin B had sufficiently quenched LY fluorescence, or whether the antibiotic had shifted the emission spectra of LY, either of which may have prevented visual detection of a small amount of fluorescent dye leaking from the pipette (LY fluorescence excitation and emission spectra were determined at 300–600 nm and 450–700 nm, respectively, at room temperature using an SLM DMX 1000 Spectrofluorometer). The presence of amphotericin B reduced LY fluorescence by $\sim 20\%$ without any significant change in its emission spectra

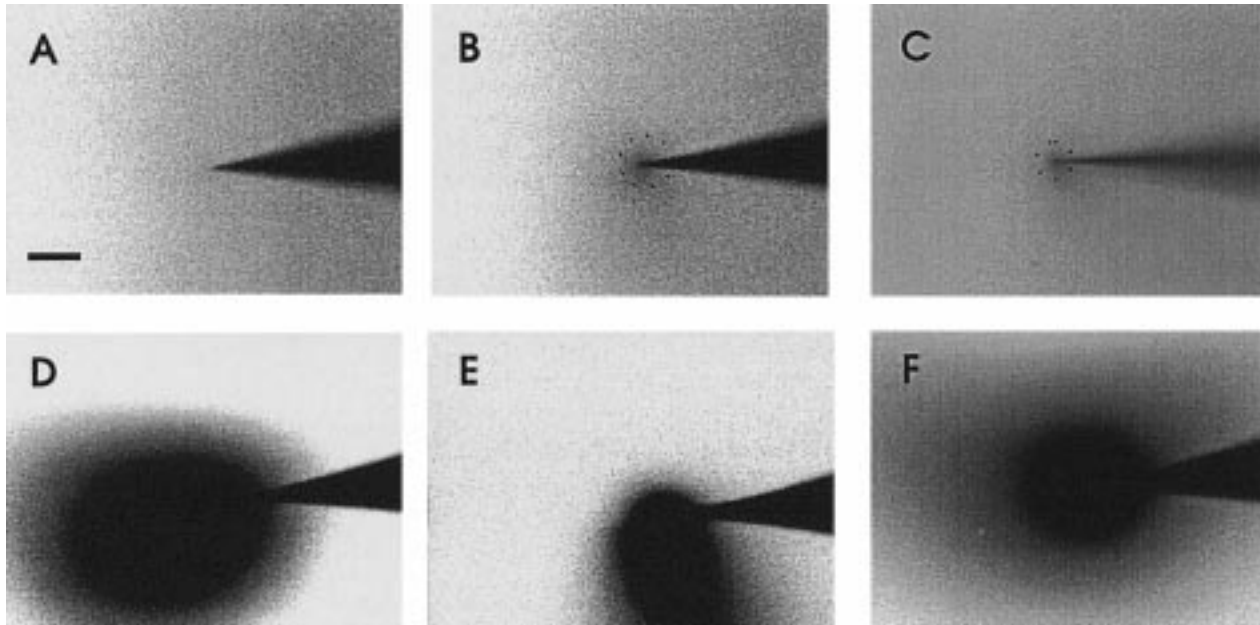


Fig. 1. (A) Non-leakage, (B,C) slow leakage, and (D-F) fast leakage of pipette solution under different conditions. In each case, ~20 mmHg of pressure was applied to the back end of the pipette. (A) Pipette solution did not leak from the patch pipette, as indicated by LY-fluorescence being confined to the pipette tip. Normal pipette solution had a greater viscosity than that used in (D-F), as evidenced by the difficulty in forcing it through the syringe filter used to fill the pipette. (B) The same pipette solution leaked slowly into ACSF from a larger pipette tip (4 µm outer diameter, 3 MΩ). (C) As in (A), except ACSF was replaced with DMSO, which caused slow leakage of amphotericin B-pipette solution from the tip. The outer diameter of the tip was <3 µm with a resistance of ~6 MΩ. (D-F) Fast leakage of pipette solution into ACSF resulted from omitting either amphotericin B (D), LY-CH dipotassium salt (E) or both amphotericin B and LY from the pipette solution (F); DMSO vehicle was still present in (D) and (F). Leakage of pipette solution was determined by excitation of LY (D); however, when testing the effect of omitting LY from the pipette solution, leakage was assessed by adding the water-soluble dye rhodamine B (E,F). The pipettes used in (A) and (C-F) had identical resistances and were produced using the same pipette puller. Scale bar=20 µm.

(not shown). This small reduction in fluorescence could not have accounted for the absence of fluorescence shown in Fig. 1A. It was concluded that amphotericin B solution was not leaking from the tip prior to forming a tight seal because LY was not observed outside of the pipette and, in addition, no extracellular deposits of LY and Biocytin were observed within the slice after tissue processing. Further, there was no evidence of whole-cell perforation due to leakage of amphotericin B into the neuropil. Leakage of amphotericin B, if it were to occur, would manifest itself by the sampled population of neurons having relatively depolarized resting membrane potentials due to whole-cell perforation^{11,29,36} compared to values measured by conventional intracellular recording (Table 1).

Tight-seal formation and rapid patch perforation

Recordings in visualized neurons: preweanlings. Despite reports to the contrary,^{4,29,36,49,51} it was determined that a tight seal was formed and maintained for 1–3 h with a cleaned, exposed soma when amphotericin B-solution was placed in the tip of the pipette. The voltage-clamp record of changes in

membrane current characterizing the cell-attached configuration and subsequent rapid perforation of the patch is shown in Fig. 2. After visually guiding the pipette on to the soma ('touch'), a seal was formed using light suction ('suck'). Too strong a suction pulse usually ruptured the patch and the recording was abandoned. If a seal formed incompletely without rupturing the patch, it was possible quickly to retract the pipette and, using a new pipette, to form a tight seal with the same neuron. It was also determined that sustained epifluorescent illumination of LY in the pipette reduced the likelihood of obtaining a successful seal, a finding that was attributed to the harmful effects on the tight-seal patch of LY excitation (see below).^{42,45} For this reason, only intermittent periods of brief epifluorescent illumination were used to check initially for LY leakage from the tip prior to seal formation, and after forming a seal, to check for integrity of the perforated patch.

Once a tight seal formed ('seal'), amphotericin B began to permeabilize the cellular patch within seconds as judged by several observations. There was a progressive increase in the amplitude of spontaneous inward action potential currents (c1-c3) followed by

Table 1. Membrane properties of solitary complex neurons in transverse tissue slices studied under different conditions (age, slice thickness and temperature) using the rapid perforated patch and conventional intracellular recording techniques

Slice preparation and conditions	V_m (mV)	AP (mV)	R_{in} (MΩ)
Preweanlings (rapid PPR)			
Thin slice (120–150 µm, P0–14, 22–25°C)	−54 ± 1 (<i>n</i> =158)	60 ± 1	747 ± 41
Thick slice (300–350 µm, P0–21, 22–25°C)	−53 ± 1 (<i>n</i> =63)	63 ± 1	721 ± 41
Weanlings and adults (rapid PRR)			
Thick slice (400 µm, ≥three weeks old, 35–37°C)	−51 ± 2 (<i>n</i> =16)	52 ± 3	213 ± 42
Adults (intracellular recording)			
Thick slice (400 µm, ≥three weeks old, 35.5–37°C), from Ref. 15	−54 ± 10 (<i>n</i> =31)	≥55	128 ± 56

V_m , resting membrane potential; AP, action potential amplitude measured from threshold to peak; R_{in} , input resistance measured from slope of the current–voltage relationship (this study) or with a constant current pulse.¹⁵

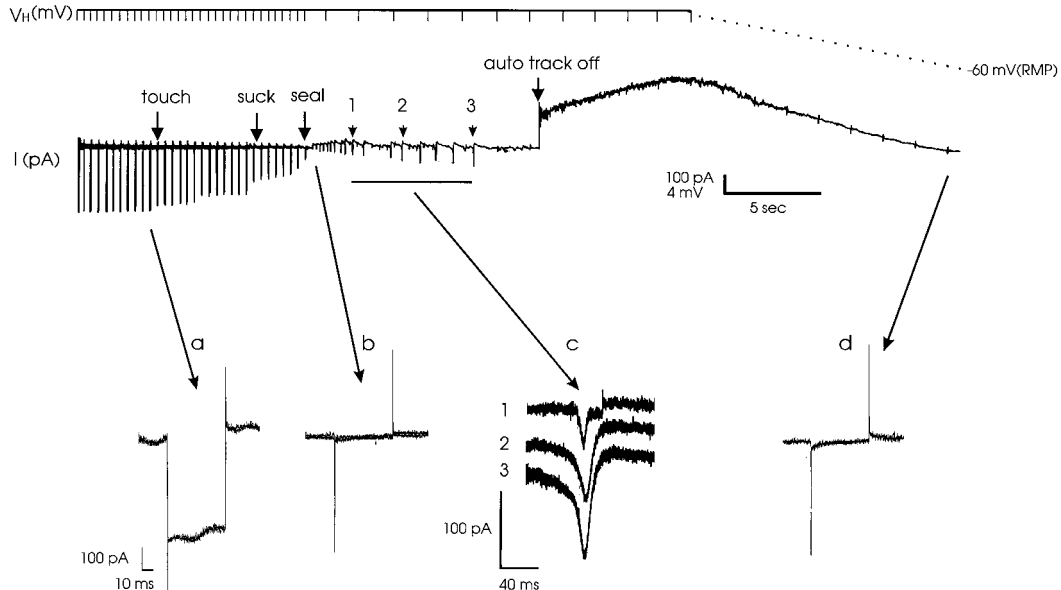


Fig. 2. Voltage-clamp record showing the changes in pipette current during tight seal formation with amphotericin B in the pipette tip, followed by changes in whole-cell current during rapid onset and steady state perforation of the cellular patch. Contact with the cell surface ('touch') was confirmed by the pipette tip dimpling the cell body concomitant with decreased pipette current. Suction applied to the pipette produced a tight seal that was indicated by pipette current decreasing from ~400 to 0 pA during a −2 mV × 25 ms voltage step (a,b). Only ~33 s was required from the time the tight seal formed (b) until the cell was clamped at V_H = −60 mV; i.e. resting membrane potential (d, RMP).

the presence of a large outward current at holding potential of 0 mV when the junction potential nulling circuitry was switched off ('auto track off'; the auto track mode on the Axopatch-1D patch clamp is activated before attempting seal formation. It automatically tracks the junction potential and maintains the pipette current at zero despite changes in pipette offset caused by the tip touching and sealing with the membrane). In addition, successful perforation was indicated by the appearance of a small inward current during a −2 mV × 25 ms voltage step (d), the series resistance decreasing to <10 MΩ, and a stable resting V_m more negative than −40 mV. In this example, as in all cases, patch perforation began immediately. By the time the amplifier was changed from voltage-clamp mode to current-clamp mode (i.e. within 1–3 min), a stable resting V_m and series

resistance were achieved, indicating that steady-state patch perforation had occurred. For example, the current– V_m relationship for the neuron in Fig. 2 was essentially unchanged after 1 h of recording from that measured immediately after steady-state perforation (see Fig. 4B). Neuronal activity usually remained constant once steady-state perforation was achieved, as indicated by resting V_m , spontaneous firing pattern, spike waveform and, as discussed in the next paper,³⁰ reproducible neuronal responses to hypercapnic acidosis. The most common source of change in the quality of recording was the unintentional rupturing of the patch (typically precipitated by injecting an excessively large depolarizing or hyperpolarizing current pulse) or reversal of perforation if the amphotericin B pipette solution was 3 h old.⁵¹

Because perforation began immediately after forming a tight seal, it was impossible to get a good measure of seal resistance. The seal was very tight, however, as indicated by the large R_{in} measured in medullary neurons compared to intracellular recordings with sharp microelectrodes (Table 1).

Blind recordings: weanlings and adults. Formation of a tight seal in brain slices from older rats, without prior cleaning and exposure of the soma, was extremely difficult. In the few cases of successful rapid PPRs, the series resistance values were higher than those in preweanlings, ranging from 7 to 98 M Ω . In general, R_{in} values were lower for blind rapid PPRs than those measured in thin and thick slices prepared from preweanlings (Table 1). Without exception, it was impossible to rupture the amphotericin B patch at the end of the experiment for loading LY and Biocytin.* Thus, it was impossible to determine whether neurons were anatomically coupled using the blind recording technique; these data will not be considered any further in the Results.

Conversion to whole-cell configuration for staining

Including the highly fluorescent dye LY in the pipette solution was useful for assessing the integrity of the amphotericin B patch during the recording session. The patch of a cleaned cell body extended $\sim 20\text{ }\mu\text{m}$ into the pipette after the tight seal was formed without any evidence of LY inside the patch or the cell body (Fig. 3B). Brief periods of epifluorescent illumination were used to visualize LY, long enough to focus the microscope and acquire a digitized CCD image. Because prolonged excitation of LY will selectively and rapidly kill the stained neuron,^{42,45} only short periods of epifluorescent illumination (2–3 s/exposure) were used. Experience showed that ~ 3 min of continuous epifluorescent illumination of LY in the pipette induced spontaneous rupturing of the patch. When care was taken to limit epifluorescent illumination during the experiment, LY (mol. wt 522) did not cross the patch and enter the cell, even when recordings lasted for up

to 3 h.[†] Refocusing below and above the pipette tip during epifluorescent illumination confirmed that dye was not leaking. At the end of recording, usually in the current-clamp mode, the patch was easily ruptured using large voltage pulses (i.e. the “zap” button on the Axopatch 1D amplifier, set at 10 ms maximum duration) and/or suction applied to the patch pipette. Rupturing of the patch was indicated by LY diffusing immediately into the neuron (Fig. 3C).

Even when epifluorescent illumination was not used to verify LY in the neuron, it was easy to predict when the patch was ruptured, by the symptomatic changes in R_{in} and membrane time-constant (τ) that transpired once intracellular washout¹⁸ and whole-cell perforation began.¹⁰ The voltage trajectories shown in Fig. 4A were produced by hyperpolarizing and depolarizing current injections at various times before (first two sets of traces) and after rupturing the patch (third and fourth sets of traces). The neuron's current– V_m relationship was unchanged during 1 h of recording (B). After going whole-cell (“1 min after rupture”), however, R_{in} decreased from 1200 to 400 M Ω and τ decreased from 65.5 to 22.4 ms (C). After 20 min of intracellular dialysis with amphotericin B solution, R_{in} and τ decreased to 93 M Ω and essentially 0 ms, respectively. In almost every case, rupturing of the patch, either spontaneously during the experiment or intentionally at the end of the experiment, precipitated an immediate reduction in R_{in} and τ that always correlated with the onset of LY staining.

Anatomical coupling

Staining lasted 20–30 min after establishing the whole-cell configuration. To withdraw the pipette from the cell body, without dislodging the cell body from the neuropil, it was necessary first to disrupt the tight seal between the pipette and the membrane. To accomplish this, several large depolarizing pulses (zap button of Axopatch 1D, 10 ms duration), alternating with brief periods of strong suction, were applied to the pipette followed by rapid withdrawal of the pipette using the micromanipulator's coarse axis of movement. LY was never observed leaking from the pipette tip after it was removed from the soma. After fixation and tissue processing, anatomical coupling was observed in 19 neurons in slices from animals between P2 and 18. Based on the number of cells sampled at each age, no significant differences were found as to when anatomical

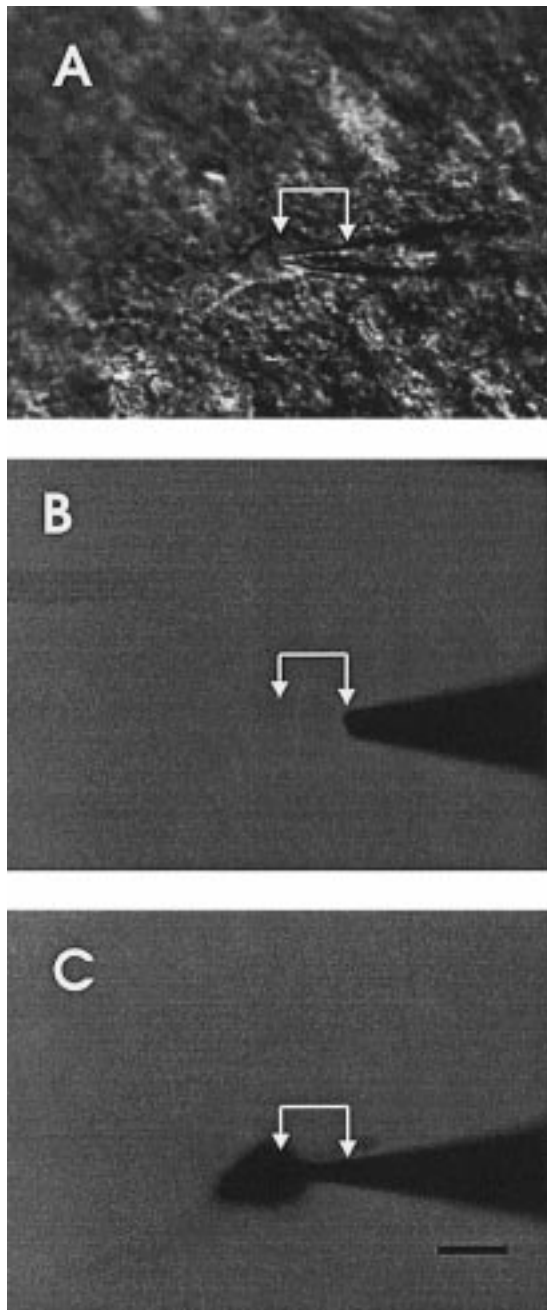
*The vacuum required to establish tight seals during blind whole-cell recordings under similar slice conditions ranges from -200 to -250 mmHg (J. B. Dean, unpublished observations), which is much higher than the vacuum used to form a tight seal with a cleaned soma.⁶⁰ It is conceivable that overlying structures are drawn into the pipette along with the cellular patch, all of which contributes to the series resistance, and impedes tight seal formation while rapid perforation of the patch is occurring. This fact, and the greater amount of cellular development in the rat brain after the second week, may explain why it was impossible to form good seals routinely, and to rupture the patch in blind rapid PPRs. Based on this study, the conventional PPR technique of layering pipette solutions is recommended for blind recordings in animals $>$ three weeks old, since it delays perforation onset until well after the seal has formed.^{4,29,36,49,51}

[†]Chung and Schlierer¹³ reported that nystatin-perforated patches were permeable to large fluorescent dyes (mol. wts 814 and 1147) and implied that nystatin does not necessarily maintain a metabolically intact cell. In their study, however, the dye-filled pipette and nystatin patch sustained multiple exposures to fluorescent illumination (≤ 10 exposures per cell) lasting 3–5 min each, which may have disturbed the integrity of the patch making it permeable to dye.

coupling was most likely to occur ($P=0.144$) (Table 2). In some cells, before removing the slice from the recording chamber for fixation, dye coupling was evident within 5 min after breaching the patch (LY transfer from the recorded cell into the adjoining cell was not continuously monitored, owing to the harmful effects of LY excitation cited above, and the unknown effects that it may have on junctional dye transfer). Altogether, of 123 neurons that stained well with LY, 79 neurons were recovered after Biocytin solidification. Of these, 55 neurons (45%) stained well, 24 neurons (19%) stained incompletely, and 44 neurons (36%) were not recovered. Dye coupling was

noted in 15 of 123 (12%) medullary neurons and tracer coupling was observed in 13 of 79 (16%) medullary neurons that were recovered. Within nuclei comprising the solitary complex, 15 of 74 (20%) the neurons recovered were anatomically coupled; 10 of 52 (19%) neurons in DMV and five of 22 (23%) neurons in NTS. Only four of 39 (10%) neurons in other areas (12 different medullary nuclei) were anatomically coupled, including: hypoglossal nucleus ($n=1$), lateral reticular nucleus ($n=2$) and medial vestibular nucleus ($n=1$). Refer also to Fig. 7 in Huang *et al.*³⁰

Three examples of dye-coupled (A,C,E,F) cell pairs in the solitary complex are shown in Fig. 5; tracer coupling is also shown for two of the cases (B,D). Anatomical coupling was usually limited to a second neuron ($n=16$) or less frequently, to a third neuron ($n=3$; e.g., see Fig. 8, below). Coupled, stained somata were separated from the neuron loaded with dye mixture by (in μm): <5–10 ($n=9$), 20–80 ($n=9$), 160–200 ($n=3$) and 1200 ($n=1$). The spatial relationship between stained cells suggested that coupling occurred by somatosomatic, dendrosomatic and/or dendrodendritic contacts. Frequently, LY-stained neural processes more completely compared to Biocytin (A–D). The intensity of Biocytin staining was typically less in the adjoining cell (D). Not all neurons ($n=4$) that were tracer coupled were also dye coupled. The two examples in Fig. 6 show where LY was confined to the recorded neuron (A,C), but Biocytin was detected in both the recorded neuron and a second neuron (B,D).



Electrotonic postsynaptic potentials

Subthreshold potentials of fairly uniform shape and amplitude, resembling ELPSPs with peak-to-

Fig. 3. (A) IR-HMC image at the surface of a 350- μm -thick slice (P12) immediately after successful perforation. The cell body of this DMV neuron was exposed and cleared of any overlying debris from the cut surface of the slice. Two arrows define the distance between the pipette tip contacting the cell body (left) and the end of the cellular patch that was pulled up into the pipette after tight seal formation (right). In this case, cellular material extended for ~20 μm into the pipette. The neuron's resting V_m was -55 mV and R_{in} was 833 M Ω . (B) The same field of view 1 h later just prior to rupturing the cellular patch, only now brief epifluorescent illumination was used to visualize the location of LY dye, which was confined to the pipette and did not cross the cellular patch and enter the neuron. Notice that the cellular patch does not contain any LY, which was indicated by the lack of LY fluorescence between the two arrows. (C) One minute after rupturing the cellular patch with alternating pulses of suction and current injection. LY-containing solution had filled the cell body and was beginning to fill dendritic processes that were coursing down into deeper levels of the slice and, therefore, were not evident in this picture. LY fluorescence can now be seen between the two arrows, indicating that the ruptured cellular patch contained the highly fluorescent dye. This neuron was not anatomically coupled to another neuron. Scale bar=20 μm .

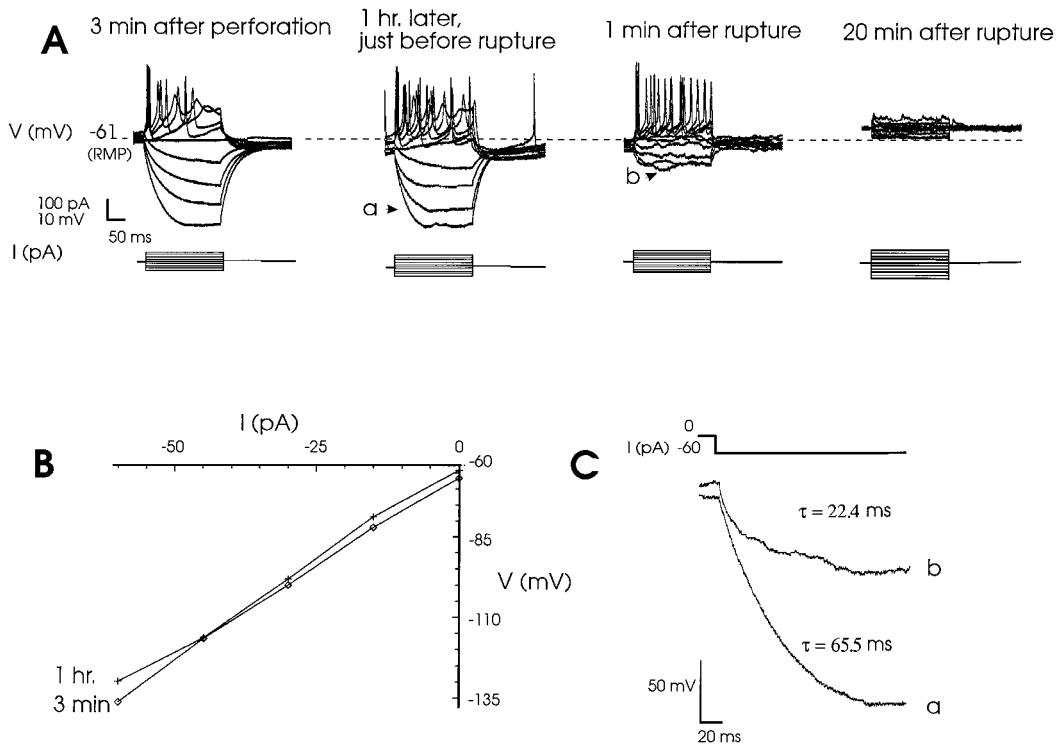


Fig. 4. (A) Changes in the current– V_m relationship and resting V_m (RMP) after intentionally rupturing the cellular patch. Pipette solution had entered the neuron within 1 min (indicated by detectable LY fluorescence, not shown), and R_m and τ both decreased, indicating that the cell was leaky owing to whole-cell perforation from the inside out. (B) Input resistance, determined from the first two sets of voltage traces presented in (A), remained constant prior to rupturing the cellular patch. (C) High gain voltage traces showing the dramatic reduction in τ that occurred immediately after rupturing the cellular patch. Traces *a* and *b* are indicated in (A). This is the same neuron that was presented above in Fig. 2 to illustrate the temporal characteristics of tight seal formation and rapid patch perforation.

Table 2. Proportion of cells sampled and the incidence of anatomical coupling at different ages in the dorsal medulla oblongata

	Postnatal age (days)				Total sample
	P1–5	P6–10	P11–15	P16–20	(N)
Proportion of neurons sampled at each age (%)	37	41	21	2	126
Proportion of anatomically coupled neurons found at different ages (%)	32	42	21	5	19

peak amplitudes of ≤ 7 mV, were observed in 11 of 19 (58%) anatomically coupled neurons in and near the solitary complex. In Fig. 7A–D, a pair of neurons can be seen in the medial vestibular nucleus, located dorsal to the NTS, whose cell bodies were ~ 7 μ m from the dorsal medullary surface and appeared to be connected by a short process (A). The recorded cell had been pruned of all other neural processes by the slicing and cleaning procedures, leaving only the cell body. The non-recorded cell had an extensive dendritic tree that projected medially towards the fourth ventricle, and ventrally and laterally within the nucleus before fading (A). The activity of the recorded cell was characterized by spontaneous action potentials and ELPSPs in high Mg^{2+} -low Ca^{2+} chemical synaptic blockade medium (C,D). As

proposed in (B), ELPSP-like activity was interpreted to be action potentials produced by “presynaptic” cell 2 that were recorded in “postsynaptic” cell 1, but were greatly reduced in amplitude owing to the voltage drop across the resistance of the gap junctions connecting the two cells. Nine anatomically coupled neurons were studied during chemical synaptic blockade; four of these neurons exhibited spontaneous ELPSPs that either first appeared ($n=2$) during chemical synaptic blockade, or were maintained during chemical synaptic blockade ($n=2$). The quality of recorded ELPSPs improved during chemical synaptic blockade, a fact that was attributed to removing the underlying conductance changes caused by neurotransmitters released from impinging chemical synapses.^{30,46}

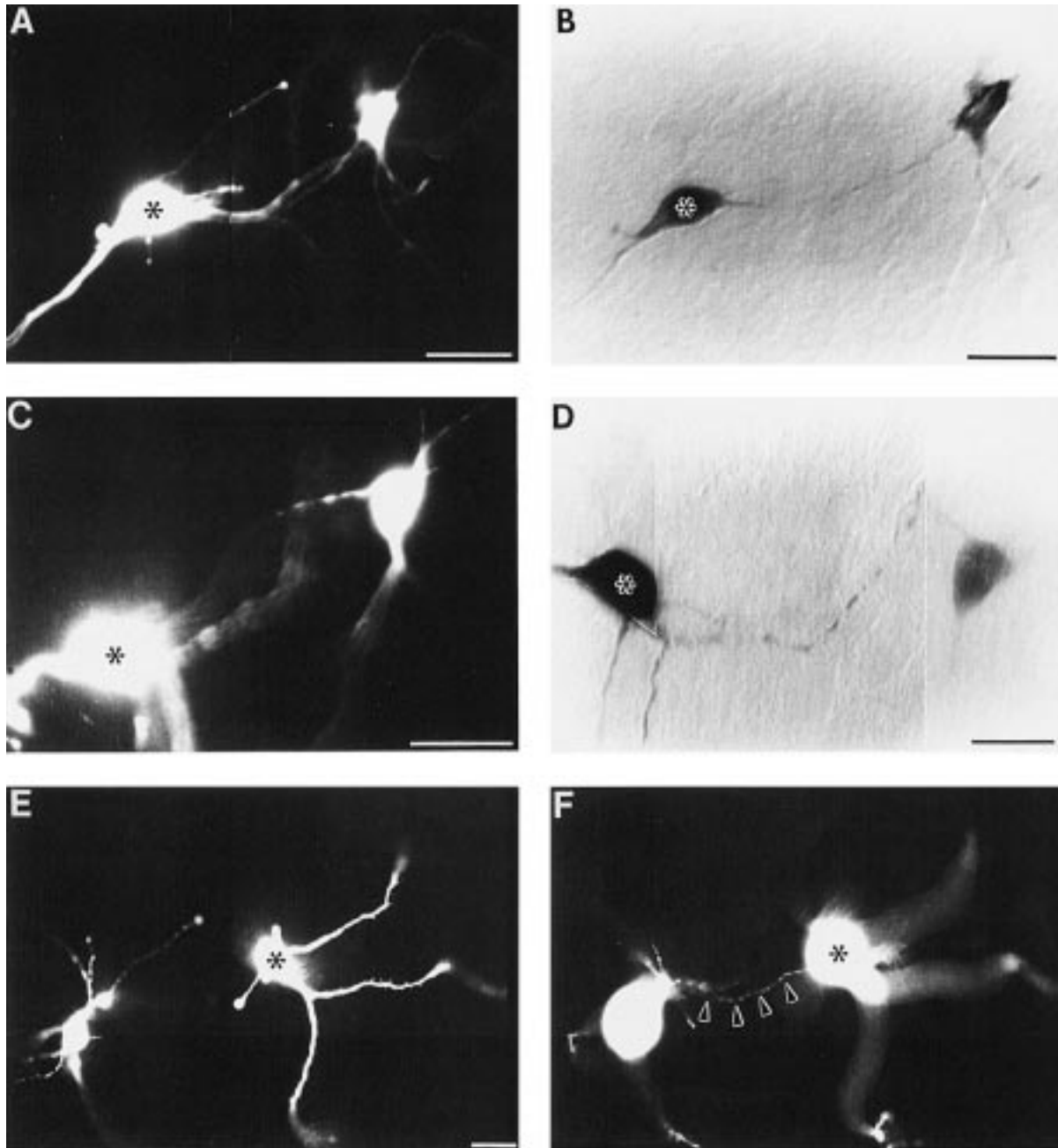


Fig. 5. Examples of anatomical coupling and double labeling in the solitary complex. (A,B) DMV neurons, P6; (C,D) NTS neurons, P10. Camera lucida reconstructions of both cell pairs are presented in Fig. 9b,e in the following paper.³⁰ (E,F) Dye-coupled neurons in the DMV, P10, shown at the same magnification, but in two different focal planes. The arrowheads in (F) show a process that appeared to be continuous between the two neurons. This cell pair was also tracer coupled (not shown). In each case, the asterisk denotes the recorded neuron initially injected with LY and Biocytin mixture. Scale bar=40 µm (A,C,E), 20 µm (B,D).

As presented in Fig. 7, detection of spontaneous ELPSP-like activity in the postsynaptic neuron depends on the presence of spontaneous firing in presynaptic neurons. In transverse brain slices superfused with ACSF, 78% of the neurons in the dorsal medulla produced action potentials at resting V_m , whereas 22% of the neurons did not. There was no significant difference in the average age of slices in

which spontaneously firing neurons and silent neurons were found: 8.1 ± 0.4 days vs 7.3 ± 0.7 days; $P=0.33$. Eighty-eight per cent of the anatomically coupled neurons were spontaneously active in ACSF, and ELPSP-like activity was detected in coupled neurons at ages P4–14.

Over half of the neurons exhibiting ELPSP-like activity (six of 11), including those neurons that had

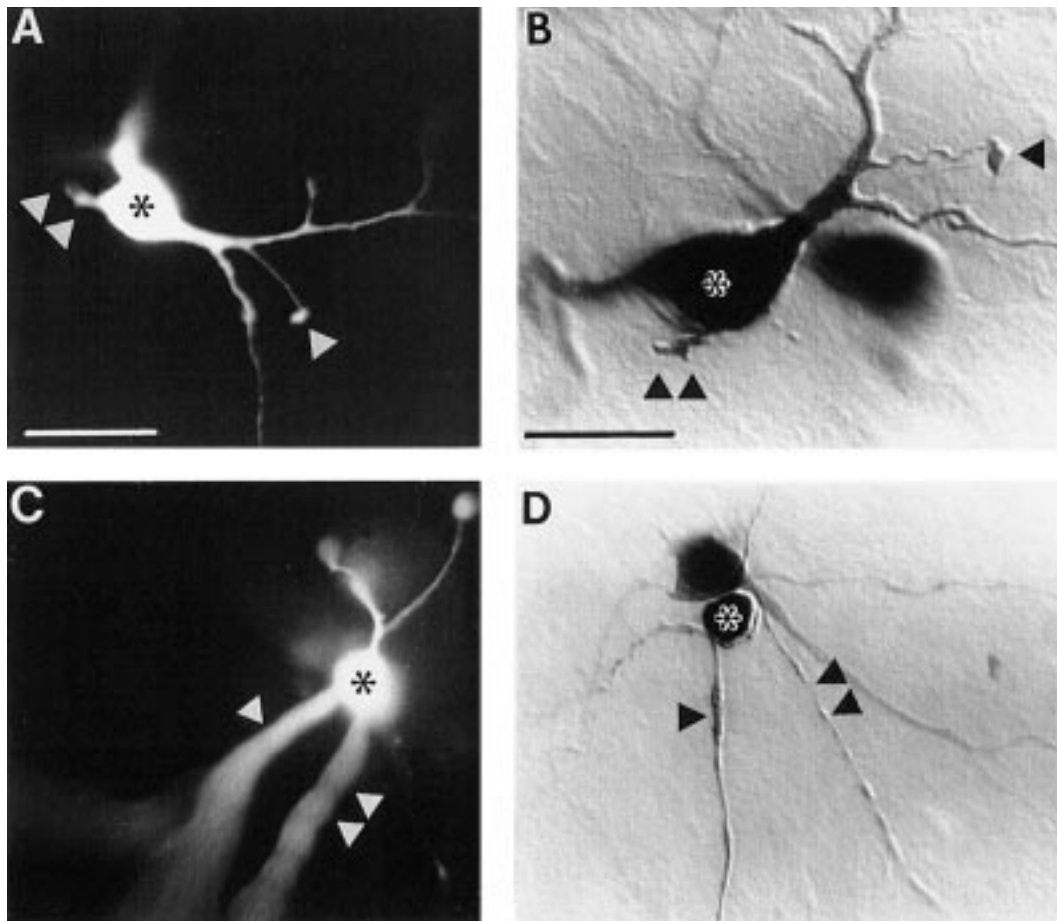


Fig. 6. Selective intercellular transfer of Biocytin and not LY from the recorded neuron (*) to a neighboring neuron. (A,B) DMV neurons, P11; (C,D) DMV neurons, P5. The triangles are points of reference since each image in a photographic pair was taken at a slightly different orientation. The out-of-focus fluorescence in (A) and (C) originates from LY-filled dendrites of the recorded neuron coursing through the slice. Scale bar=50 μm (A), 25 μm (C).

the largest amplitude ELPSPs, were either directly apposed (e.g., Figs 6B, 7A), or their somata were separated by $\leq 10 \mu\text{m}$. ELPSPs were also detected in neurons separated from their anatomically coupled neighbor by 20–200 μm ($n=5$; e.g., Fig. 5C,D). The spatial geometry of neurons demonstrating measurable ELPSPs suggested somasomatic coupling and/or dendrosomatic coupling. Neurons that appeared to be coupled primarily by dendrodendritic contacts, however, usually showed no evidence of ELPSPs ($n=4$; e.g., Fig. 5E,F), or those that could be measured at the cell body were extremely small ($n=1$; Fig. 8A). Three tracer-coupled neurons located in the ventral aspect of DMV are shown in Fig. 8. Dendrites of recorded cell 1 projected medially and intermingled with dendrites of a partially stained second cell, while a faintly stained third cell was observed making an apparent dendrosomatic contact with the second cell. High gain traces of the V_m record of cell 1 revealed small biphasic waveforms of uniform shape and amplitude that resembled an ELPSP (B, enclosed area). Not all neurons that were adjacent to each other

displayed ELPSPs. Three pairs of anatomically coupled neurons, separated by $\leq 10 \mu\text{m}$, did not exhibit ELPSP-like activity ($n=3$; e.g., Fig. 6C,D).

Sustained depolarization and hyperpolarization of the recorded cell increased and decreased, respectively, the frequency of ELPSPs (Fig. 9). In this example, as in Fig. 7, the spatial relationship of the two cell bodies suggested that they were coupled by somasomatic or somadendritic connections. Likewise, the recorded cell was pruned of its dendritic processes by slicing and did not fire spontaneously. Rapid depolarization by current injection induced action potentials and ELPSPs (B); however, slower onset, sustained depolarizing current injection increased the periodicity of ELPSPs without evoking action potentials (C).

A summary of the temporal characteristics of ELPSPs in the dorsal medulla observed in anatomically coupled neurons in preweanlings is given in Fig. 10. Notice the similarity between the duration and polarity of ELPSPs and action potentials recorded in the same neuron (A). In several neurons, ELPSPs

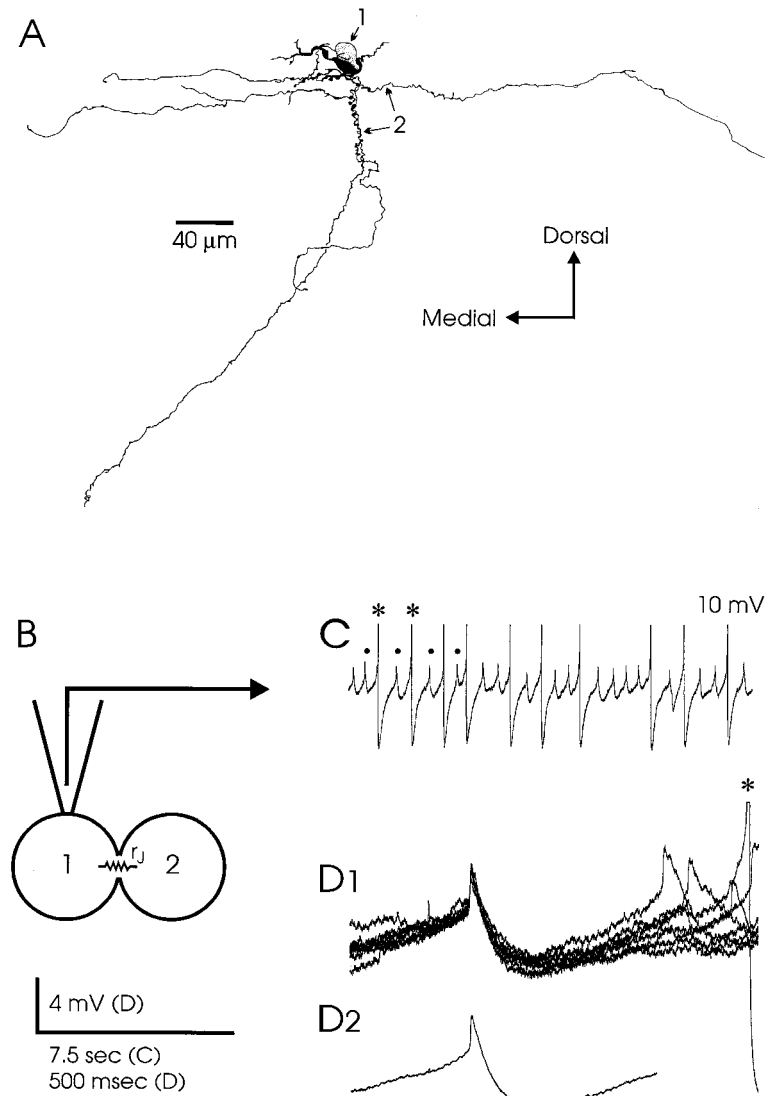


Fig. 7. Spontaneous ELPSPs in an anatomically coupled neuron located in the dorsal medulla (P5). (A) Camera lucida reconstruction of the tracer-coupled cell pair. The two neurons were also dye coupled (not shown). Cell 1 was the recorded neuron. (B) Proposed model of electrotonic coupling between the two neurons using a single pipette recording configuration; r_j , gap junctional resistance. (C) Spontaneous ELPSPs (●) and truncated action potentials (*) during high Mg^{2+} -low Ca^{2+} chemical synaptic blockade. (D) Seven superimposed ELPSPs during chemical synaptic blockade (1) and the resulting average ELPSP (2).

coincided with the prepotential of the action potential with a result similar to that of an excitatory postsynaptic potential (B). ELPSPs were smaller in amplitude when they occurred during the afterhyperpolarization of the recorded cell due to the increased outward conductances known to transpire during this period (C). The biphasic nature and time-course of the ELPSP were similar to action potentials, but were considerably different from inhibitory (C,D) and excitatory postsynaptic potentials (not shown; however, see Fig. 11).

The presence of cell-cell coupling in the vicinity of the solitary complex of mature rats was not determined in this study. This was because the

patch could not be ruptured after rapid PPR in weanlings and adults to load the cell with dye mixture. Furthermore, because of the extremely low success rate of establishing a tight seal in these slices (Table 1), not many experiments were attempted using older animals. However, as stated in the Introduction, one of the reasons for initiating this study was an earlier observation of ELPSP-like activity in the solitary complex of weanling and adult rats while using the blind whole-cell recording technique (unpublished data from Dean and Reddy¹⁸). An example of ELPSP-like activity in the adult is presented in Fig. 11 for the purpose of comparison with ELPSP-like activity in

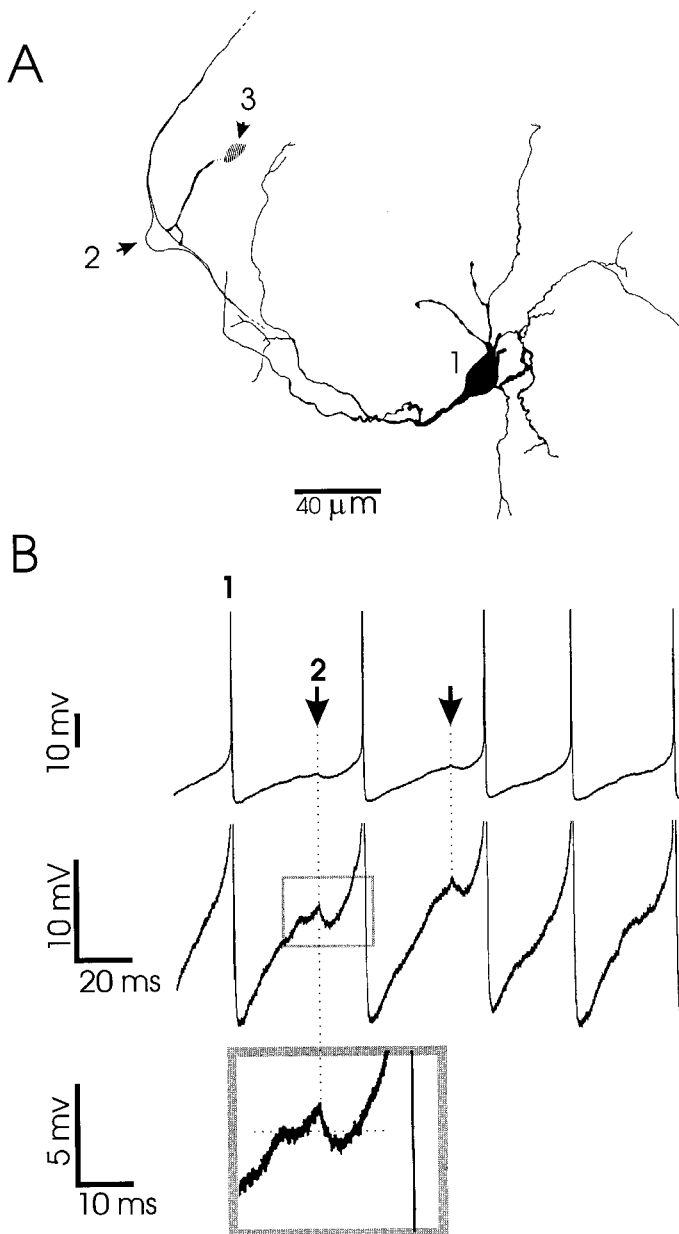


Fig. 8. (A) Camera lucida reconstruction of three tracer-coupled neurons in the DMV (P10). These neurons were not dye coupled. (B) High gain record of V_m in ACSF was characterized by action potentials (1) and small, biphasic potentials (2) resembling ELPSPs.

anatomically coupled neurons in preweanlings. An example of spontaneous ELPSP-like activity with a peak-to-peak amplitude of ~ 10 mV is shown in Fig. 11A. This type of activity was detected in $< 10\%$ of the blind whole-cell recordings in solitary complex neurons in slices prepared from older rats. It was not determined whether neurons exhibiting ELPSPs were anatomically coupled; however, the small waveforms resembled ELPSPs recorded in preweanlings. Spontaneous biphasic waveforms had a peak-to-peak amplitudes of ≤ 10 mV, with the positive phase having a shorter duration than

chemical excitatory synaptic potentials (B,D). In addition, ELPSPs frequently coincided with the prepotential of the action potential (C,D), a situation that was also observed in preweanlings (cf. Fig. 10B).

DISCUSSION

Anatomical coupling

Dye and tracer coupling have been reported in several brainstem nuclei including nucleus ambiguus,³⁷ hypoglossal nucleus,⁴³ inferior olive,⁸

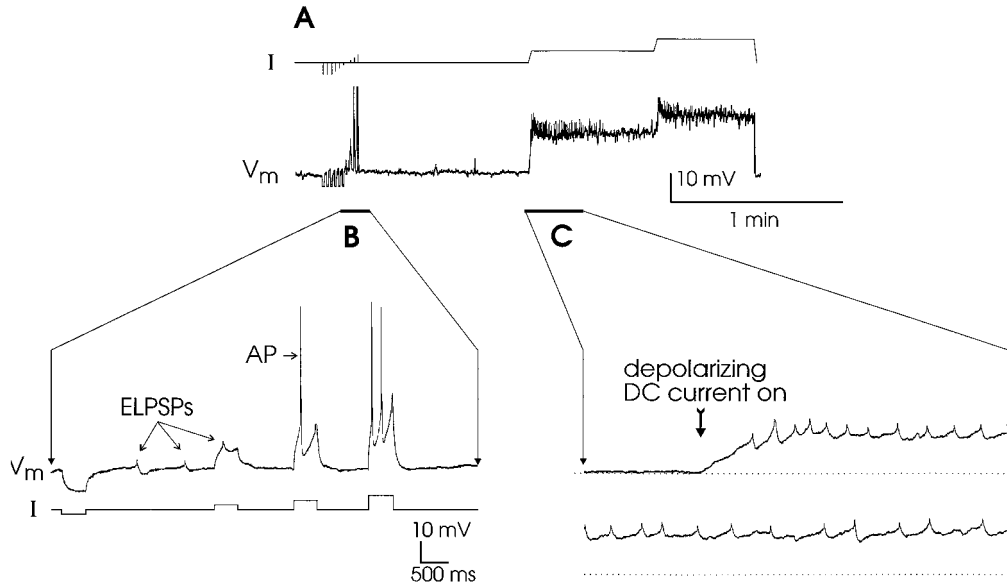


Fig. 9. (A–C) ELPSP-like activity increased in frequency during depolarization of the recorded neuron. This NTS neuron (P7) was anatomically coupled to a second neuron with three primary processes; however, the recorded cell had been pruned of all its neural processes. In (C), the two traces are continuous in time. The dotted line indicates resting V_m during sustained depolarizing current injection. AP, action potential; I, relative changes in holding current beginning at zero pA. Records in (A–C) were acquired during high Mg^{2+} -low Ca^{2+} chemical synaptic blockade.

dorsal raphe⁶⁴ and locus coeruleus.^{11,66} Likewise, dendrodendritic gap junctions were identified in the NTS and medullary reticular formation in mice (P5–20)⁵⁰ and inferior olive in adult cat.⁶¹ This study is the first report, however, of anatomical coupling in the solitary complex. Moreover, it provides the first evidence for anatomical coupling in mammalian brain slices under conditions that greatly reduce potential sources of staining artifacts (artifacts reviewed in the Appendix in Ref. 3). Anatomical coupling and ELPSP-like activity (see below) were highly correlated, suggesting that both phenomena occurred by intercellular transfer of current, LY and/or Biocytin through the same gap junctions. The potential functional significance of cell–cell coupling in the solitary complex and adjacent regions of the dorsal medulla is the subject of the following paper,³⁰ which reports a high incidence of cell–cell coupling in neurons that are hypothesized to function as central chemoreceptors for the respiratory and cardiovascular control systems.

Because of the microscopy and recording techniques used in this study, the incidence of anatomical coupling was not overestimated. There are two reasons, however, why it is believed that the incidence and extent of anatomical coupling were underestimated: severing of points of coupling in the transverse brain slice, and the possibility of weak electrotonic coupling between neurons in the dorsal medulla. Transverse brain slices were employed in this study to correlate morphological findings with other studies by this laboratory using the same slice preparation.^{16,18,57} Although a portion of the den-

dritic tree in NTS and DMV neurons was maintained in transverse slices,^{16,30} other dendrites, oriented along the longitudinal axis of the dorsal medulla, were severed.^{6,7,22,32} Consequently, points of dendrodendritic and dendrosomatic coupling between neurons along the longitudinal axis of the dorsal medulla were disrupted.³⁰ Travagli *et al.*⁶⁶ found that the dendritic arborizations and incidence of cell–cell coupling in locus coeruleus neurons were greater in horizontal slices than in transverse slices. Similarly, coupling may be better preserved in the dorsal medulla in a horizontal or sagittal slice that does not compromise longitudinally oriented dendrites in the solitary complex.

The presence of dye coupling also correlates directly with the strength of electrotonic coupling and not the presence or absence of electrotonic coupling.⁴⁶ Likewise, tracer coupling may be determined by the strength of electrotonic coupling, although this has yet to be determined. There are reports of the absence of dye coupling between cells identified to be electrotonically coupled^{5,55} and ionically coupled.⁴⁰ In these cases, it was proposed that LY was not observed in the second cell either because its molecular size prevented it from crossing the gap junction or, alternatively, because the gap junction had a low permeability for LY so that not enough fluorescent dye accumulated in the adjoining cell(s) for visual detection.^{5,40,43,48,55,67} If electrotonic coupling between solitary complex neurons was weak, as is hypothesized below, then the use of LY (and Biocytin?) would not detect every instance of anatomical coupling.

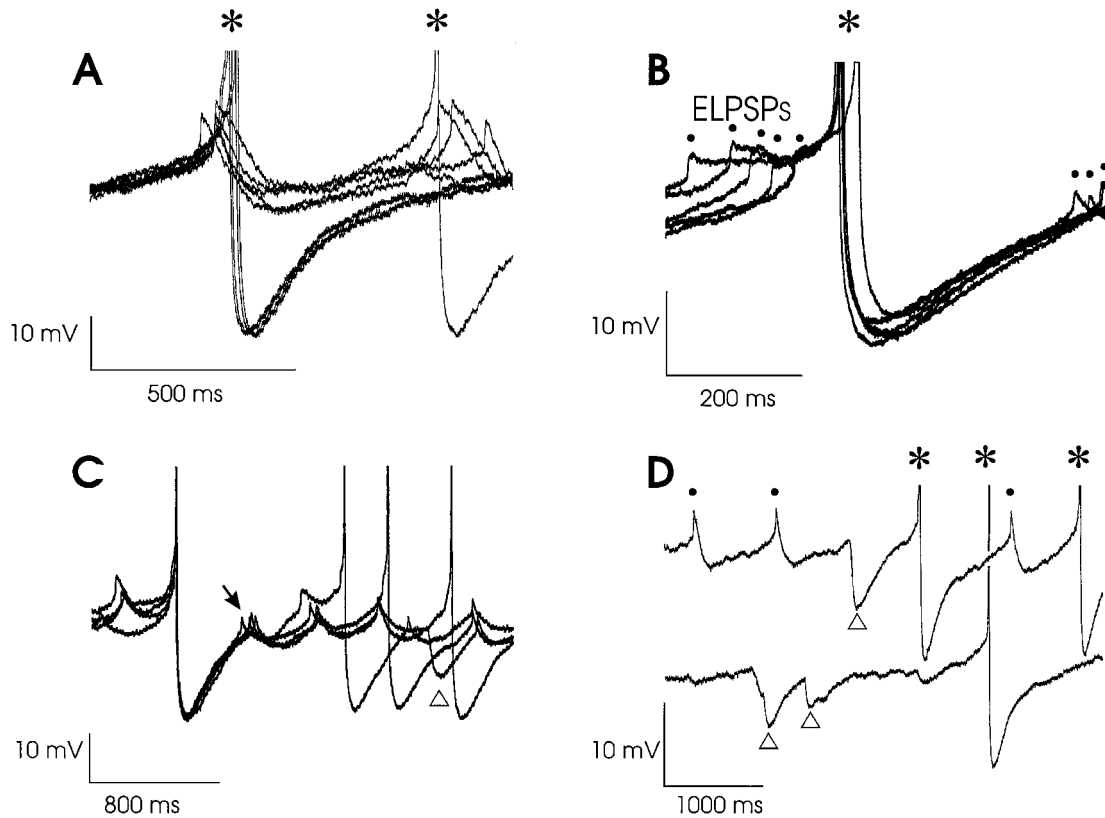


Fig. 10. (A) Superimposed ELPSPs and action potentials (*, truncated) recorded in an anatomically coupled neuron (P5) during chemical synaptic blockade (11.4 mM Mg²⁺-1.2 mM Ca²⁺; spontaneous inhibitory postsynaptic potentials were reduced in frequency, but not not completely eliminated in this example). Both ELPSPs and action potentials had similar time-courses. (B) ELPSPs (●) similar to the fast prepotentials described in Refs 23 and 41. As shown here, action potentials were sometimes preceded by a ELPSP that summed with the prepotential. (C) Spontaneous ELPSPs were observed during the afterhyperpolarization (arrow). Notice the difference in the waveforms between the ELPSP and an inhibitory postsynaptic potential (△). (D) Comparison of the time-course of ELPSPs (●), action potentials (*, truncated) and inhibitory postsynaptic potentials (△).

Several anatomically coupled neurons in the dorsal medulla were tracer coupled without any indication of being dye coupled. Comparisons between biotinylated tracers and LY show that the biotinylated tracers detect a higher incidence, and greater extent of anatomical coupling, than LY.^{43,48,67} Differences in junctional permeability between these stains could be due to the larger molecular size of LY compared with the biotinylated tracers. Alternatively, the gap junction may have a lower permeability for LY than Biotin so that not enough fluorescent dye accumulates in the adjoining coupled neurons for visual detection.^{5,40,43,48,55,67} Such differences in permeability could result from the differences in charge between LY (negative charge)⁶³ and biotinylated tracer (positive charge).²⁸ Further, fluorescent stains such as LY could be more difficult to detect in the adjoining cells than are the biotinylated tracers, which use molecular amplification procedures to increase the amount of visible tracer end product.^{28,68}

Previous intracellular staining studies of neurons in NTS and DMV have not detected dye^{7,19,22,52} or tracer coupling.^{7,31,33} There are three possible reasons for these negative results. This was the first demonstration of anatomical coupling in the mammalian CNS using a pipette solution containing amphotericin B. It is conceivable that there is an unidentified effect of amphotericin B at gap junctions that increases permeability for LY and Biotin compared to internal solutions without amphotericin B.^{6,7,19,31,33,52} Secondly, the strength and/or amount of electrotonic coupling can decrease with age,²⁵ which in turn, reduces^{11,48} or abolishes⁴³ anatomical coupling in the CNS. Previous studies of the solitary complex typically used tissue slices from older animals.^{7,19,22,33,52} In the present study, anatomical coupling was observed through at least P18, an age when the rat is ready to be weaned. Owing to the small number of neurons sampled after P14, it was not determined how common, if at all, cell-cell coupling is after the second week of life. Regarding this issue, it was notable that ELPSP-like activity was observed

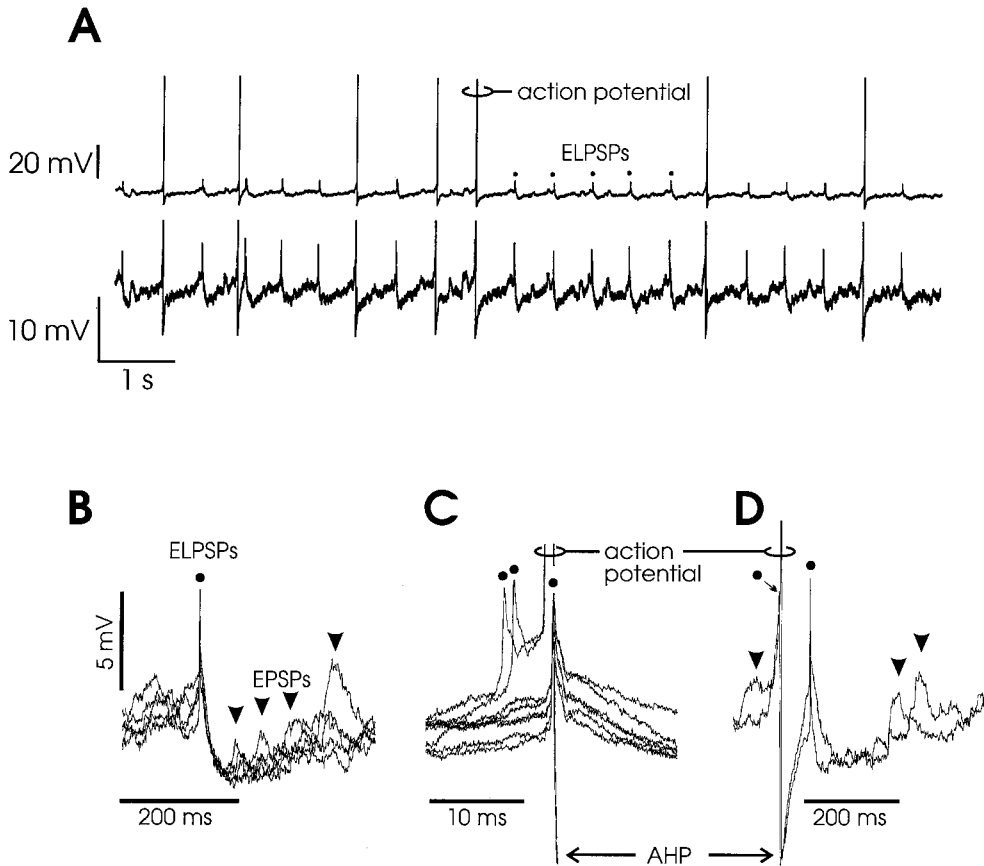


Fig. 11. Spontaneous ELPSP-like activity in the NTS of a 400- μm -thick transverse slice prepared from adult rat. Membrane potential was measured at $\sim 37^\circ\text{C}$ in ACSF using a conventional whole-cell recording technique as described in Dean and Reddy.¹⁸ (A) Low gain (top) and high gain (bottom) traces of V_m showing action potentials and presumptive ELPSPs (●). (B–D) High gain, superimposed records of ELPSPs (●), excitatory postsynaptic potentials (EPSPs, ▼), and action potentials (AHP, afterhyperpolarization of the action potential) recorded from the same neuron presented in (A). (B) Five traces; (C) eight traces; (D) two traces.

in a small percentage of neurons in the solitary complex of mature rats during whole-cell recording, suggesting that cell-cell coupling is present in the adult. The extent of coupling in the fully developed dorsal medulla, however, is unknown.

Finally, previous studies may have missed tracer coupling in the solitary complex because too little biotinylated tracer was injected into the recorded neuron. A sufficient quantity of tracer must be injected into the recorded neuron to allow ample accumulation of tracer in the coupled neuron(s) for visual detection (this would also apply to LY). The amount of dye loaded into the neuron will be determined by the initial concentration of dye placed into the pipette and the duration of iontophoresis. The present study used up to 0.5% solution of Biocytin with 20–30 min of loading. In contrast, earlier studies using similar concentrations of tracer used shorter periods of iontophoresis, which would reduce the amount of tracer loaded into the recorded cell. This may have precluded visual detection of tracer coupling in slices prepared from neonates,³¹ juveniles and adults.^{7,33}

Electrotonic coupling

The strongest evidence that anatomical coupling denotes electrotonic coupling in the vicinity of the solitary complex was obtained by observing ELPSP-like activity in over half of the neurons that were dye and/or tracer coupled. Neurons that were not anatomically coupled did not show any evidence of electrotonic synaptic transmission. It could not be confirmed in this study that subthreshold potentials were ELPSPs since only one recording pipette was used; however, they exhibited characteristics that strongly suggested their origin to be in a neuron electrotonically coupled to the recorded neuron. Other investigators have observed similar ELPSP-like activity in dye-coupled neurons using single and paired recordings, the latter experiments revealing that these small waveforms were indeed ELPSPs. Previous studies have referred to electrotonic synaptic activity as fast potentials,²³ fast depolarizing potentials,^{27,70} fast prepotentials,^{23,41} coupling potentials^{23,70} and short latency depolarizations.^{35,38,39}

It has been proposed that ELPSP-like activity was unrelated to electrotonic coupling and resulted

from other non-junctional phenomena including dendritic spikes⁵⁹ and ephaptic interactions (i.e. electrical field effects).^{20,53,54} Such potential sources of ELPSP-like activity seem unlikely in the present study given the high correlation between ELPSPs and anatomical coupling. Moreover, in the case of two neurons, ELPSPs were recorded from a cell body essentially devoid of *all* neuronal processes, but that was coupled to an intact neuron, thereby ruling out dendritic spikes as a source of sub-threshold potentials. In addition, previous studies^{53,54} that reported waveforms believed to be due to ephaptic interactions have required differential recordings (i.e. intracellular potential minus extracellular potential), which were not made in the present study.

When spontaneous ELPSP-like activity was identified during the experiment it was 100% accurate in predicting dye and/or tracer coupling afterwards. None the less, not all neurons that were anatomically coupled displayed ELPSP-like activity. ELPSPs, however, would not be measured if the adjoining cell was not spontaneously firing action potentials. Twenty-two per cent of the neurons recorded in dorsal medullary slices were not spontaneously active at resting V_m . Moreover, ELPSPs may have gone undetected in anatomically coupled neurons that were not studied in high Mg^{2+} -low Ca^{2+} medium because they were lost in the background chemical synaptic activity.⁴⁶ Blockade of chemical synaptic activity tended to improve the signal-to-noise ratio of the ELPSPs,³⁰ and in two cases, uncovered ELPSPs that were not apparent in ACSF. It is also possible that ELPSPs originating in distal neural processes were reduced in amplitude by the cable properties of the postsynaptic neuron. The small amplitude of the ELPSP suggests that the magnitude of junctional currents flowing through these gap junctions is relatively small, which would make it difficult to detect electrotonic activity. Rash and co-workers⁵⁶ have shown that the majority of gap junctions in the mammalian spinal cord is comprised of fewer connexions compared with non-neuronal cells, suggesting weak electrotonic coupling at this level of the CNS. Likewise, any neurons in the dorsal medulla that were weakly coupled through dendrodendritic gap junctions would result in immeasurably small ELPSPs at the cell body. Thus, as suggested by the present study, ELPSPs would most probably be detected in neurons that were coupled by somatosomatic and somadendritic contacts (which were inferred solely by the proximity of somata and processes between labeled neurons). Thus, distal sites of coupling, conductance changes associated with impinging chemical synapses, and lack of spontaneous firing in presynaptic neurons may partly explain the disparity between the high incidence of dye coupling and the low incidence of electrophysiological evidence for cell-cell coupling in earlier studies using mammalian brain slices.^{1,20,23,34,38,41,43}

Rapid perforated patch technique

Placing amphotericin B directly in the pipette tip allowed rapid perforation of the patch so that electrophysiological data could be collected within a few minutes of patching on to a neuron. The combination of amphotericin B and LY in the tip produced a hydrophobic, viscous pipette solution that resisted flow through a small pipette opening submerged in ACSF. It is possible that there was minimal leakage of pipette solution into the bath whose concentration of LY was below the threshold for visible detection. This seems unlikely, however, since there was no evidence of amphotericin B leakage, which would have rapidly increased membrane conductance and depolarized the neuron.^{29,36} The absence of any detectable leakage of pipette solution may also explain why, unlike previous studies,^{4,29,36,49,51} tight seals formed routinely with antibiotic in the tip. Based on the findings reported here, any previous attempts to patch cells with amphotericin B in the tip, without LY, would have resulted in leakage of pipette solution into the neuropil. Given the quickness with which amphotericin B begins to perforate the membrane (see also Ref. 51), it seems likely that the cell would begin to perforate before the pipette was placed against it. Hence, the problem may not be that antibiotic *in the tip* interferes with tight seal formation,^{49,51} but rather, that antibiotic *leaked from the tip* begins to perforate the membrane. This, in turn, may interfere with formation of a seal between the pipette and membrane.

Why does the amphotericin B-LY mixture not leak into the neuropil? Amphotericin B is insoluble in water near pH 7, and amphotericin B-DMSO stock solution forms into micelles when mixed with internal solution that are dispersed by ultrasonication. Similarly, small micelles would form again inside the tip at the interface between amphotericin B solution and ACSF (a water-based solution). When ACSF was replaced with DMSO, a solution that amphotericin B is soluble in, pipette solution began to leak from the tip. Leakage was slow, however, indicating that other factors besides the hydrophobicity of amphotericin B were impeding flow through the tip. These additional factors were determined to be the resistance imposed by the pipette tip opening and the presence of LY-CH dipotassium salt in the tip. Typically, lower concentrations of LY and biotinylated tracer are used to stain the neuron during whole-cell recording compared to intracellular recordings with sharp microelectrodes.⁹ For rapid PPR, a LY concentration ranging from 0.15–0.5% solution was adequate for preventing leakage of pipette solution and for visualizing LY in the pipette in the presence of amphotericin B, which reduced LY fluorescence by 20%. It is unclear why LY contributed to non-leakage when mixed with amphotericin B, but it may be related to the high concentration of salt present in the tip in association with the hydrophobic

ionophore. It is possible that LY could be substituted for a less costly, non-fluorescent compound if it is not necessary to identify dye coupling.

Once the patch was ruptured at the end of the experiment, the neuron stained rapidly with LY despite the high viscosity of the pipette solution. The reason for rapid staining is unclear. It may be related to the lipid components of the tight-seal patch, which include plasmalemmal vesicles and lipid bilayers within the membrane.^{58,60} The ultrastructural changes in the ruptured tight-seal patch are unknown. Exposure of any of these lipid components to the patch pipette solution, however, would provide a substrate in which the lipophilic solution was soluble, enabling dye mixture to flow into the neuron.

Nystatin, another popular ionophore used for conventional PPR,^{4,29} was not tried, so it is unknown whether this antibiotic behaves similarly to amphotericin B when mixed with LY. In other experiments, not shown here, rapid PPRs were possible using the ionophore gramicidin.³⁶ Gramicidin-pipette solution was less viscous than amphotericin B-pipette solution and leaked into the bath when positive pressure was applied to the pipette. Without positive pressure though, pipette solution did not leak. Thus, caution must be used to avoid potential non-junctional staining with the mixture of gramicidin, LY and Biocytin in the tip.

Successful seal formation and rupturing of the patch for introducing dye mixture required that the soma was exposed. Thus, for brain slices, the use of

the rapid PPR technique is restricted to neurons that are easily visualized and readily cleaned; i.e. brain slices prepared from immature animals.^{21,65} Because the incidence of cell-cell coupling decreases or disappears in some mammalian CNS nuclei during development,^{25,43,48} it will be important in the future to conduct parallel studies in slices prepared from older animals using conventional intracellular recording and staining techniques under blind conditions.^{2,9,23,70} Despite the difficulty of these types of experiments and the possibility of non-junctional staining, they are currently the only way to establish cell-cell coupling in the adult CNS. However, when combined with the methods reported here for preweanlings, it provides a powerful approach to studying cell-cell coupling in the mammalian CNS.

Acknowledgements—We would like to thank Dr Albert Berger and colleagues for their assistance initially with the thin slice technique and infrared video microscopy. We are also grateful to Ms Leslie Spencer for her technical assistance, Mr Mike Shade (Fryer Company, Cincinnati, OH) for his help in developing the IR-HMC system, Dr Jim Kramer for making the spectrofluorimetry measurements, Dr Robert Fyffe for his guidance in developing the Biocytin technique, and Drs John Rash and Richard White for reviewing earlier drafts of this manuscript. This work was supported by NIH Grant HL46308 and NSF Grant IBN9296087 (JBD), the W.S.U. Research Challenge Program (JBD), an American Heart Association–Ohio Affiliate Fellowship MV-94-06-F (JSE), and W.S.U. Biomedical Sciences Ph.D. Program (TLS).

REFERENCES

1. Alger B. E., McCarren M. and Fisher R. S. (1983) On the possibility of simultaneously recording from two cells with a single microelectrode in the hippocampal slice. *Brain Res.* **270**, 137–141.
2. Andrew R. D., MacVicar B. A., Dudek F. E. and Hatton G. I. (1981) Dye transfer through gap junctions between neuroendocrine cells of rat hypothalamus. *Science* **211**, 1187–1189.
3. Andrew R. D., Taylor C. P., Snow R. W. and Dudek F. E. (1982) Coupling in rat hippocampal slices: dye coupled transfer between CA1 pyramidal cells. *Brain Res. Bull.* **8**, 211–222.
4. Armstrong D. L. and White R. E. (1992) An enzymatic mechanism for potassium channel stimulation through pertussis-toxin-sensitive G proteins. *Trends Neurosci.* **15**, 403–408.
5. Audesirk G., Audesirk T. and Bowsher P. (1982) Variability and frequent failure of lucifer yellow to pass between two electrically coupled neurons in *Lymnaea stagnalis*. *J. Neurobiol.* **13**, 369–375.
6. Barber W. D., Yuan C. S., Burks T. F., Feldman J. L. and Greer J. J. (1995) *In vitro* brainstem–gastric preparation with intact vagi for study of primary visceral afferent input to dorsal vagal complex in caudal medulla. *J. auton. nerv. Syst.* **51**, 181–189.
7. Barnes K. L., McQueeney A. J., Barrett W. R. and Knowles W. D. (1994) Morphology and projections of Neurobiotin-labeled nucleus tractus solitarius neurons recorded *in vitro*. *Brain Res. Bull.* **34**, 339–348.
8. Benardo L. S. and Foster R. E. (1986) Oscillatory behavior in inferior olive neurons: mechanism, modulation, cell aggregates. *Brain Res. Bull.* **17**, 773–784.
9. Blanton M. G., Lo Turco J. J. and Kriegstein A. R. (1989) Whole cell recording from neurons in slices of reptilian and mammalian cerebral cortex. *J. Neurosci. Meth.* **30**, 203–210.
10. Cass A., Finkelstein A. and Krespi V. (1970) The ion permeability in thin lipid membranes by polyene antibiotics nystatin and amphotericin B. *J. gen. Physiol.* **56**, 100–124.
11. Christie M. J. and Jelinek H. F. (1993) Dye coupling among neurons of the rat locus coeruleus during postnatal development. *Neuroscience* **56**, 129–137.
12. Christie M. J., Williams J. T. and North R. A. (1989) Electrical coupling synchronizes subthreshold activity in locus coeruleus neurons *in vitro* from neonatal rats. *J. Neurosci.* **9**, 3584–3589.
13. Chung I. and Schlichter L. C. (1993) Criteria for perforated-patch recordings: ion currents versus dye permeation in human T lymphocytes. *Pflügers Arch.* **424**, 511–515.
14. Cunningham M. G. and McKay R. D. G. (1993) A hypothermic miniaturized stereotaxic instrument for surgery in newborn rats. *J. Neurosci. Meth.* **47**, 105–114.
15. Dean J. B., Bayliss D. A., Erickson J. T., Lawing W. L. and Millhorn D. E. (1990) Depolarization and stimulation of neurons in nucleus tractus solitarius by carbon dioxide does not require chemical synaptic input. *Neuroscience* **36**, 207–216.

16. Dean J. B., Huang R.-Q. and Fyffe R. E. W. (1995) Anatomically coupled CO₂/H⁺-chemosensitive neurons in the dorsal medulla. *Soc. Neurosci. Abstr.* **21**, 1883.
17. Dean J. B. and Millhorn D. E. (1992) CO₂-induced depolarization of neurons in nucleus tractus solitarii: a potential substrate for central chemoreceptors. In *Cardiorespiratory and Motor Coordination* (eds Koepchen H. P. and Huopaniemi T.), pp. 53–59. Springer, Berlin.
18. Dean J. B. and Reddy R. B. (1995) Effects of intracellular dialysis on CO₂/H⁺ chemosensitivity in brainstem neurons. In *Ventral Brainstem Mechanisms and Control of Respiration and Blood Pressure, Lung Biology in Health and Disease* (eds Trout C. O., Millis R. M., Kiwull-Schöne H. F. and Schläfke M. E.), Vol. 82, pp. 453–461. Marcel Dekker, New York.
19. Dekin M. S., Getting P. A. and Johnson S. M. (1987) *In vitro* characterization of neurons in the ventral part of the nucleus tractus solitarius. I. Identification of neuronal types and repetitive firing properties. *J. Neurophysiol.* **58**, 195–214.
20. Dudek F. E. and Snow R. W. (1985) Electrical interactions and synchronization of cortical neurons: electrotonic coupling and field effects. In *Gap Junctions* (eds Bennett M. V. L. and Spray D. C.), pp. 325–336. Cold Spring Harbor Laboratory Press, New York.
21. Edwards F. A., Konnerth A., Sakmann B. and Takahashi T. (1989) A thin slice preparation for patch clamp recordings from neurones of the mammalian central nervous system. *Pflügers Arch.* **414**, 600–612.
22. Fox E. A. and Powley T. L. (1992) Morphology of identified preganglionic neurons in the dorsal motor nucleus of the vagus. *J. comp. Neurol.* **322**, 79–98.
23. Grace A. A. and Bunney B. S. (1983) Intracellular and extracellular electrophysiology of nigral dopaminergic neurons—3. Evidence for electrotonic coupling. *Neuroscience* **10**, 333–348.
24. Grace A. A. and Llinás R. (1985) Morphological artifacts induced in intracellularly stained neurons by dehydration: circumvention using rapid dimethyl sulfoxide clearing. *Neuroscience* **16**, 461–475.
25. Green C. R. (1992) The role of gap junctions during development and patterning. In *Fundamentals of Medical Cell Biology, Developmental Biology* (ed. Edward E.), Vol. 7, pp. 133–149. JAI Press, Greenwich, CT.
26. Hatton G. I. and Yang Q. Z. (1996) Synaptically released histamine increases dye coupling among vasopressinergic neurons of the supraoptic nucleus: mediation by H₁-receptors and cyclic nucleotides. *J. Neurosci.* **16**, 123–129.
27. Hatton G. I., Yang Q. Z. and Cobbett P. (1987) Dye coupling among immunocytochemically identified neurons in the supraoptic nucleus: increased incidence in lactating rats. *Neuroscience* **21**, 923–930.
28. Horikawa K. and Armstrong W. E. (1988) A versatile means of intracellular labeling: injection of Biocytin and its detection with avidin conjugates. *J. Neurosci. Meth.* **25**, 1–11.
29. Horn R. and Marty A. (1988) Muscarinic activation of ionic currents measured by a new whole-cell recording method. *J. gen. Physiol.* **92**, 145–159.
30. Huang R.-Q. and Erlichman J. S. and Dean J. B. (1997) Cell-cell coupling between CO₂-excited neurons in the dorsal medulla oblongata. *Neuroscience* **80**, 41–57.
31. Kalia M., Schweitzer P., Champagnat J. and Denavit-Saubie M. (1993) Two distinct phases characterize maturation of neurons in the nucleus of the tractus solitarius during early development: morphological and electrophysiological evidence. *J. comp. Neurol.* **327**, 37–47.
32. Kaneko A., Nishimura Y., Tauchi M. and Shimai K. (1981) Morphological observation of retinal cells presumably made syncytial by an electrode penetration. *J. Neurosci. Meth.* **4**, 299–303.
33. King M. S. and Bradley R. M. (1994) Relationship between structure and function of neurons in the rat rostral nucleus tractus solitarii. *J. comp. Neurol.* **344**, 50–64.
34. Knowles W. D., Funch P. G. and Schwartzkroin P. A. (1982) Electrotonic and dye coupling in hippocampal CA1 pyramidal cells *in vitro*. *Neuroscience* **7**, 1713–1722.
35. Korn H., Sotelo C. and Crepel F. (1973) Electrotonic coupling between neurons in the rat lateral vestibular nucleus. *Expl Brain Res.* **16**, 255–275.
36. Kyrozis A. and Reichling D. B. (1995) Perforated-patch recording with gramicidin avoids artifactual changes in intracellular chloride concentration. *J. Neurosci. Meth.* **57**, 27–35.
37. Lewis D. I. (1994) Dye coupling between vagal motoneurones within the compact region of the adult rat nucleus ambiguus, *in-vitro*. *J. auton. nerv. Syst.* **47**, 53–58.
38. Llinás R. (1985) Electrotonic transmission in the mammalian central nervous system. In *Gap Junctions* (eds Bennett M. V. L. and Spray D. C.), pp. 337–353. Cold Spring Harbor Laboratory Press, New York.
39. Llinás R. and Yarom Y. (1981) Electrophysiology of mammalian inferior olfactory neurones *in vitro*. Different types of voltage-dependent ionic conductances. *J. Physiol., Lond.* **315**, 549–567.
40. Lo C. W. and Gilula N. B. (1979) Gap junctional communication in the post-implantation mouse embryo. *Cell* **18**, 411–422.
41. MacVicar B. A. and Dudek F. E. (1982) Electrotonic coupling between granule cells of rat dentate gyrus: physiological and anatomical evidence. *J. Neurophysiol.* **47**, 579–592.
42. Marder E. (1984) Roles of electrical coupling in neural circuits as revealed by selective neuronal deletions. *J. exp. Biol.* **112**, 147–167.
43. Mazza E., Nunez-Abades P. A., Spielmann J. M. and Cameron W. E. (1992) Anatomical and electrotonic coupling in developing genioglossal motoneurons of the rat. *Brain Res.* **598**, 127–137.
44. Metz C. B., Schneider S. P. and Fyffe R. E. W. (1989) Selective suppression of endogenous peroxidase activity: application for enhancing appearance of HRP-labeled neurons *in vitro*. *J. Neurosci. Meth.* **26**, 181–188.
45. Miller J. P. and Selverston A. I. (1979) Rapid killing of single neurons by irradiation of intracellularly injected dye. *Science* **206**, 702–704.
46. Murphy D. A., Hadley R. D. and Kater S. B. (1983) Axotomy-induced parallel increases in electrical and dye coupling between identified neurons of *Helisoma*. *J. Neurosci.* **3**, 1422–1429.
47. Nicoll R. A. and Madison D. V. (1982) General anesthetics hyperpolarize neurons in the vertebrate central nervous system. *Science* **217**, 1055–1057.
48. Peinado A., Yuste R. and Katz L. C. (1993) Extensive dye coupling between rat neocortical neurons during the period of circuit formation. *Neuron* **10**, 102–114.

49. Pickering T. E. and Spanswick D. and Logan S. D. (1993) Whole-cell patch-clamp recording from neurones in spinal cord slices. In *Electrophysiology, A Practical Approach* (ed. Wallis D. I.), pp. 169–188. Oxford University Press, Oxford.
50. Quattrochi J. J., Madison R., Kljavin I. J. and Marsala J. and Kosik K. S. (1986) Integrative structural correlates of central respiratory rhythmicity: a new hypothesis. In *Neurobiology of the Control of Breathing* (eds von Euler C. and Lagercrantz H.), pp. 231–241. Raven Press, New York.
51. Rae J., Cooper K., Gates P. and Watsky M. (1991) Low access resistance perforated patch recordings using amphotericin B. *J. Neurosci. Meth.* **37**, 15–26.
52. Ragganbass M., Sharpak S., Dubois-Dauphin M. and Dreifuss J. J. (1988) Electrophysiological evidence for oxytocin receptors on neurones located in the dorsal motor nucleus of the vagus nerve in the rat brainstem. *J. Receptor Res.* **8**, 273–282.
53. Raminsky M. (1980) Ephaptic transmission between single nerve fibers in the spinal nerve roots of dystrophic mice. *J. Physiol. Lond.* **305**, 151–169.
54. Ramon F. and Morre J. W. (1978) Ephaptic transmission in squid giant axons. *Am. J. Physiol.* **234**, C162–169.
55. Ransom B. R. and Kettenmann H. (1990) Electrical coupling, without dye coupling, between mammalian astrocytes and oligodendrocytes in cell culture. *Glia* **3**, 258–266.
56. Rash J. E., Dillman R. K., Bilhartz B. L., Duffy H. S., Whalen L. R. and Yasumura T. (1996) Mixed synapses discovered and mapped throughout mammalian spinal cord. *Proc. natn. Acad. Sci. U.S.A.* **93**, 4235–4239.
57. Ritucci N. A., Erlichman J. S., Dean J. B. and Putnam R. W. (1996) A fluorescence technique to measure intracellular pH of single neurons in brainstem slices. *J. Neurosci. Meth.* **68**, 149–163.
58. Ruknudin A., Song M. J. and Sachs F. (1991) The ultrastructure of patch-clamped membranes: a study using high voltage electron microscopy. *J. Cell Biol.* **112**, 125–134.
59. Schwartzkroin P. A. (1975) Characteristics of CA1 neurons recorded intracellularly in the hippocampal *in vitro* slice preparation. *Brain Res.* **85**, 23–436.
60. Sokabe M. and Sachs F. (1990) The structure and dynamics of patch-clamped membranes: a study using differential interference contrast light microscopy. *J. Cell Biol.* **111**, 599–606.
61. Sotelo C., Llinás R. and Baker R. (1974) Structural study of inferior olivary nucleus of the cat: morphological correlates of electrotonic coupling. *J. Neurophysiol.* **37**, 541–559.
62. Spray D. C. and Bennett M. V. L. (1985) Physiology and pharmacology of gap junctions. *A. Rev. Physiol.* **47**, 281–303.
63. Stewart W. W. (1978) Functional connections between cells as revealed by dye coupling with a highly fluorescent naphthalimide tracer. *Cell* **14**, 741–759.
64. Stezhka V. V. and Lovick T. A. (1995) Dye coupling between dorsal raphe neurones. *Expl Brain Res.* **105**, 383–390.
65. Stuart G. J., Dodt H.-U. and Sakmann B. (1993) Patch-clamp recordings from the soma and dendrites of neurons in brain slices using infrared video microscopy. *Pflügers Arch.* **423**, 511–518.
66. Travagli R. A., Wessendorf M. and Williams J. T. (1996) Dendritic arbor of locus coeruleus neurons contributes to opioid inhibition. *J. Neurophysiol.* **75**, 2029–2035.
67. Vaney D. I. (1991) Many types of retinal neurons show tracer coupling when injected with Biocytin or Neurobiotin. *Neurosci. Lett.* **125**, 187–190.
68. Vaney D. I. (1992) Photochromic intensification of diaminobenzidine reaction product in the presence of tetrazolium salts: applications for intracellular labelling and immunohistochemistry. *J. Neurosci. Meth.* **44**, 217–223.
69. Waxman S. G., Waxman M. and Pappas G. D. (1980) Coordinated micropinocytotic activity of adjacent neuronal membranes in mammalian central nervous system. *Neurosci. Lett.* **20**, 141–146.
70. Yang Q. Z. and Hatton G. I. (1988) Direct evidence for electrical coupling among rat supraoptic nucleus neurons. *Brain Res.* **463**, 47–56.

(Accepted 7 January 1997)